

AIR FORCE REPORT NO.
SAMSO-TR-72-209

AEROSPACE REPORT NO.
TR-0073(S3450-60)-1

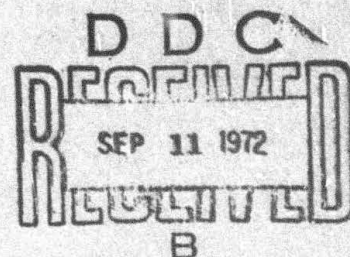
AD 748292

Laminar, Transitional, and Turbulent Heat Transfer Measurements on a Yawed Blunt Conical Nosetip

Prepared by G. F. WIDHOPF
Technology Division

72 SEP 01

San Bernardino Operations
THE AEROSPACE CORPORATION



Prepared for SPACE AND MISSILE SYSTEMS ORGANIZATION
AIR FORCE SYSTEMS COMMAND
LOS ANGELES AIR FORCE STATION
Los Angeles, California

Reproduced by
NATIONAL TECHNICAL
INFORMATION SERVICE
U.S. Department of Commerce
Springfield VA 22151

APPROVED FOR PUBLIC RELEASE:
DISTRIBUTION UNLIMITED

48R

UNCLASSIFIED

Security Classification

DOCUMENT CONTROL DATA - R & D

(Security classification of title, body of abstract and indexing annotation must be entered when the overall report is classified)

1. ORIGINATING ACTIVITY (Corporate author)
The Aerospace Corporation
El Segundo, California

4a. REPORT SECURITY CLASSIFICATION
Unclassified

2b. GROUP

3. REPORT TITLE
LAMINAR, TRANSITION, AND TURBULENT HEAT TRANSFER
MEASUREMENTS ON A YAWED BLUNT CONICAL NOSETIP

4. DESCRIPTIVE NOTES (Type of report and inclusive dates)

5. AUTHOR(S) (First name, middle initial, last name)

George F. Widhopf

6. REPORT DATE

72 SEP 01

7a. TOTAL NO. OF PAGES

85

7b. NO. OF REFS

30

8a. CONTRACT OR GRANT NO.

F04701-72-C-0072

8b. ORIGINATOR'S REPORT NUMBER(S)

TR-0073(S3450-60)-1

h. PROJECT NO.

9b. OTHER REPORT NO(S) (Any other numbers that may be assigned this report)

SAMSO-TR-72-209

10. DISTRIBUTION STATEMENT

Approved for public release; distribution unlimited

11. SUPPLEMENTARY NOTES

12. SPONSORING MILITARY ACTIVITY

Space and Missile Systems Organization
Air Force Systems Command
Los Angeles, California

13. ABSTRACT

nose radius *free stream conditions* *times 10 to the 6th power*

Laminar, transitional, and turbulent heat-transfer rates measured on a blunt ($R_N = 2.5$ in.) 9-deg half-angle cone in a $M_\infty = 5$ air flow at various angles of attack are presented. Measurements were made at nominal free-stream Reynolds numbers of 48.5, 19, 11, and 4.6 (10^6) per foot at nominal angles of attack $\alpha = 0^\circ, 5^\circ, 10^\circ, 15^\circ, 20^\circ$, and 27° . The wall-to-stagnation temperature ratio varied between 0.20 and 0.29. Detailed circumferential ($\Delta\theta = 30^\circ$) and axial ($S/R_N = 5-25$) distributions of both the heat transfer rate and surface pressure were obtained over the entire model at each test condition and angle of attack. Natural transition occurred on the hemispherical cap near the stagnation region at the $Re_\infty = 48.5$ and 19 (10^6) test conditions. Heat transfer rates computed along inviscid surface streamlines using various heat transfer formulations are compared to the data. The Vaglio-Laurin type turbulent heat transfer formulations are shown to be in good agreement with the data at all test conditions, while those formulations which use reference rather than edge conditions to define the local rate substantially overpredict the turbulent heat transfer rate over the entire surface. The applicability of the angle-of-attack heat transfer correlation, which had been previously proposed by the author, is demonstrated for the present test results for both the laminar and turbulent flow conditions.

ia

UNCLASSIFIED

Security Classification

UNCLASSIFIED

Security Classification

14.

KEY WORDS

Laminar Heat Transfer

Turbulent Heat Transfer

Blunt Cone at Angle of Attack

Distribution Statement (Continued)

Abstract (Continued)

ik

UNCLASSIFIED

Security Classification

**Air Force Report No.
SAMSO-TR-72-209**

**Aerospace Report No.
TR-0073(S3450-60)-1**

**LAMINAR, TRANSITIONAL, AND TURBULENT HEAT TRANSFER
MEASUREMENTS ON A YAWED BLUNT
CONICAL NOSETIP**

**Prepared by
G. F. Widhopf
Technology Division**

72 SEP 01

**San Bernardino Operations
THE AEROSPACE CORPORATION
El Segundo, California**

**Prepared for
SPACE AND MISSILE SYSTEMS ORGANIZATION
AIR FORCE SYSTEMS COMMAND
LOS ANGELES AIR FORCE STATION
Los Angeles, California**

**Approved for public release;
distribution unlimited**

ic

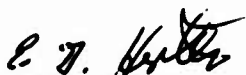
FOREWORD

This report is published by The Aerospace Corporation, El Segundo, California, under Air Force Contract No. F04701-71-C-0172.

This report documents research carried out from September 1970 to January 1972. The pressure tests were conducted in December 1970 and the heat transfer tests were conducted in February 1971. The report was submitted for review and approval on 14 July 1972 to Lieutenant Colonel Donald R. Shover, RSSE.

The author wishes to acknowledge the very capable assistance of Robert Hall who supervised the entire test program at the Naval Ordnance Laboratory (NOL). The assistance of Mary Ellen Falusi (NOL) in reducing the wind tunnel data and the assistance of Rita Harriman (Aerospace Corp.) in the organization and plotting of the final data is also gratefully acknowledged. Thanks are extended to Ken Reed (Aerospace Corp.) for his efficient coding and running of the streamline tracing program and to Frank Fernandez (Aerospace Corp.) who originally suggested this work.

Approved



E. G. Hertler, Associate Director
Applied Mechanics and Physics
Subdivision
Technology Division
San Bernardino Operations



R. A. Hartunian, Director
Reentry Systems Division
Development Operations

Publication of this report does not constitute Air Force approval of the report's findings or conclusions. It is published only for the exchange and stimulation of ideas.



D. R. Shover, Lt Col, USAF
Chief, Environmental Technology Div.
Deputy for Reentry Systems

ABSTRACT

Laminar, transitional, and turbulent heat-transfer rates measured on a blunt ($R_N = 2.5$ in.) 9-deg half-angle cone in a $M_\infty = 5$ air flow at various angles of attack are presented. Measurements were made at nominal free-stream Reynolds numbers of 48.5, 19, 11, and $4.6(10)^6$ per foot at nominal angles of attack $\alpha = 0^\circ, 5^\circ, 10^\circ, 15^\circ, 20^\circ$, and 27° . The wall-to-stagnation temperature ratio varied between 0.20 and 0.29. Detailed circumferential ($\Delta\phi \approx 30^\circ$) and axial ($S/R_N \leq 5.25$) distributions of both the heat transfer rate and surface pressure were obtained over the entire model at each test condition and angle of attack. Natural transition occurred on the hemispherical cap near the stagnation region at the $Re_\infty = 48.5$ and $19(10)^6$ test conditions. Heat transfer rates computed along inviscid surface streamlines using various heat transfer formulations are compared to the data. The Vaglio-Laurin type turbulent heat transfer formulations are shown to be in good agreement with the data at all test conditions, while those formulations which use reference rather than edge conditions to define the local rate substantially overpredict the turbulent heat transfer rate over the entire surface. The applicability of the angle-of-attack heat transfer correlation, which had been previously proposed by the author, is demonstrated for the present test results for both the laminar and turbulent flow conditions.

CONTENTS

FOREWORD	ii
ABSTRACT	iii
NOMENCLATURE	vii
I. INTRODUCTION	1
II. EXPERIMENTAL FACILITY AND TEST CONDITIONS	3
III. MODEL CONFIGURATION AND INSTRUMENTATION	5
IV. EXPERIMENTAL RESULTS	9
V. COMPARISON WITH NUMERICAL RESULTS	27
VI. HEAT TRANSFER CORRELATIONS	41
A. Turbulent Case	42
B. Laminar Case	44
VII. SUMMARY AND CONCLUSIONS	49
APPENDIX A. TEST CONDITIONS AND DATA TABULATIONS	51
APPENDIX B. DATA REDUCTION TECHNIQUE	73
APPENDIX C. THOMAS-FITZSIMMONS CONDUCTION CORRECTION METHOD	81
REFERENCES	83

Preceding page blank

FIGURES

1.	Schematic of Model and Instrumentation Locations	6
2.	Surface Pressure Distributions Along the Windward and Leeward Rays at Various Angles of Attack	10
3.	Heat Transfer Distributions Along the Windward and Leeward Rays at Various Angles of Attack	11
4.	Heat Transfer Distribution on the Hemispherical Cap	16
5.	Smooth Wall Transition Data on Blunt Nosetips	20
6.	Heat Transfer Variation with Angle of Attack at Various Stations Along the Windward and Leeward Rays	21
7.	Comparison Between Experimental and Calculated Circumferential Turbulent Heat Transfer Distributions at Station $S/R_N = 5.25$ for Various Angles of Attack	24
8.	Circumferential Variation of the Heat Transfer at Various Stations on the Hemisphere	26
9.	Comparison Between the Experimental and Calculated Heat Transfer Distributions at $\alpha = 0^\circ$; $Re_\infty = 18.3(10)^6$	31
10.	Comparison Between the Experimental and Calculated Longitudinal Heat Transfer Distributions on the Conical Surface	32
11.	Comparison Between the Experimental and Calculated Circumferential Pressure Distributions on the Conical Surface	35
12.	Pressure Distribution on the Hemispherical Cap	39
13.	Correlation of the Turbulent Heat Transfer Data at Stations $S/R_N = 2, 3.5, \text{ and } 5.25$	43
14.	Correlation of the Laminar Heat Transfer Data at Stations $S/R_N = 2, 3.5, \text{ and } 5.25$	45

NOMENCLATURE

A	defined by Eq. (5a)
C_p	specific heat
H	total enthalpy
H_r	recovery enthalpy
h	heat transfer coefficient = $q_w / (T_r - T_w)$, static enthalpy
h₂	length element which characterizes the spreading of the streamlines
l	length element along a streamline as measured from the most forward point on the surface
M	Mach number
P	nondimensionalized pressure, p/p_0
P_r	Prandtl number (a value of 0.716 was used exclusively)
p	static pressure
q	heat transfer per unit area per unit time
q_{cw}	cold wall heat transfer rate
Re	Reynolds number per foot
R_N	nose radius
S	surface coordinate
T	temperature
U	velocity
α	angle of attack
δ	wall thickness
ϵ	defined by Eq. (5a)

μ	coefficient of viscosity
ν	kinematic viscosity, μ/ρ
ρ	density
ϕ	circumferential angle measured from leeward ray

Subscripts

e	boundary layer edge conditions
m	model material
o	laminar stagnation point condition
se	boundary layer edge stagnation conditions
w	wall
∞	freestream conditions
1, 3, 4	reference conditions used in Eqs. (2), (3) and (4), respectively, which are defined using Eqs. (5b)

I. INTRODUCTION

Verification of the accuracy of any proposed numerical method of calculating the heat transfer rate to the surface of a hypersonic reentry vehicle invariably depends upon its subsequent agreement with experimental data. This becomes even more pertinent when three dimensional transitional and turbulent flows are considered. At present, there is a need for angle-of-attack heat transfer data wherein the flow undergoes a natural transition from the laminar to the turbulent state on the blunt portion of the nosetip at a location close to the stagnation region. It is especially desirable to achieve the fully turbulent state near the sonic point so that measurements of the peak heating can be obtained. In this regard, detailed measurements over the entire region encompassing the first few nose radii are needed. Also, since most reentry conditions are characterized by low wall-to-stagnation temperature ratios, the test conditions should also adequately simulate this parameter. The simulation of these conditions will then provide a good experimental data base which can then be used to determine the accuracy of the various proposed numerical methods. The need for an accurate determination of which numerical scheme best approximates the actual situation and the resulting impact on the important problems of thermal protection and shape change resulting from surface ablation is obvious.

Previous investigations have not adequately simulated all of these conditions. In Ref. 1 an extensive investigation of the fully turbulent heat transfer rate on the conical surface of a blunt cone at various angles of attack was presented. Unfortunately, in that study the spherical cap had to be roughened in order to sustain the turbulent flow and prevent the flow from relaminarizing. Thus, the heat transfer rates on the hemisphere could not be obtained. Reference 2 includes a study of the leeward plane heat transfer distribution at angle of attack.

This report presents the results of a test program wherein the previously outlined conditions were simulated. Heat transfer and static pressure distributions measured on the surface of a blunt cone at various angles of attack are presented at four different freestream conditions. The results of some numerical calculations of the turbulent heat transfer rate, utilizing various (five) methods proposed in the literature, are compared to the data. The applicability of an angle-of-attack heat transfer correlation,³ which had been previously proposed by the author, is also investigated for both the laminar and turbulent flow cases.

II. EXPERIMENTAL FACILITY AND TEST CONDITIONS

The test program was conducted in the U. S. Naval Ordnance Laboratory Hypersonic Tunnel 8 Facility. A complete description of this open-jet, blow-down facility and its performance capabilities is contained in Refs. 4 and 5. The present measurements were made in an air environment at a freestream Mach number of 5 and at nominal freestream Reynolds numbers of 48.5, 19, 11 and $4.6(10)^6$ per foot. The model was cooled with liquid nitrogen and the resulting wall-to-stagnation temperature ratio obtained using this procedure varied between $0.20 \leq T_w/T_o \leq 0.29$. The nominal angles of attack considered included $\alpha = 0^\circ, 5^\circ, 10^\circ, 15^\circ, 20^\circ$, and 27.5° . A tabulation of the test conditions is included in Appendix A.

III. MODEL CONFIGURATION AND INSTRUMENTATION

The configuration utilized was a spherically capped ($R_N = 2.5$ in.) 9-degree half-angle cone. Two models were fabricated for use in this test program. A thick wall ($\delta = 0.187$ in.) model was constructed of brass and used during the pressure measurement phase of the program. The heat transfer model consisted of a thin wall shell ($\delta = 0.025$ in., nominal) fabricated of ARMCO 17-4PH stainless steel. After fabrication, the surface was heat treated to condition H-1150 and polished to an 8 micron finish. Webs were used for internal support and are shown in the sketch of the heat transfer model (Fig. 1). As can be seen from this figure, the webs were positioned so that they would not interfere with or influence the measurements. Both the surface pressure (95 gages) and heat transfer (73 gages) were measured at each freestream condition previously described, at approximately eleven axial stations ($S/R_N = 0.15, 0.30, 0.45, 0.60, 0.75, 0.90, 1.05, 1.30, 1.50, 2.0, 3.5, 5.25$), along seven circumferential rays ($\phi = 0^\circ, 40^\circ, 70^\circ, 90^\circ, 120^\circ, 150^\circ, \text{ and } 180^\circ$). The locations of both types of instrumentation are shown in Fig. 1.

The heat transfer measurements were made utilizing 0.005 in. diameter chromel-alumel thermocouples, whose responses were automatically recorded by the NOL high speed data acquisition system.⁶ The resulting data were then reduced using the calorimeter technique described in Refs. 7 and 8 and corrected for initial transient conduction errors using the method of Ref. 9. A description of the data reduction technique is included in Appendix B.* Possible sources of error were examined and are also discussed in this Appendix. The heat transfer coefficient, h , was directly determined from the thermocouple output and subsequently corrected for initial transient conduction errors. The data presented herein is in terms of the cold wall heat transfer rate, q_{cw} , defined as $q_{cw} = hT_{se}$.

*The specific test procedures used in this experimental program and the data reduction technique are also described in Ref. 10.

Preceding page blank

The pressure measurements were made utilizing surface pressure taps connected to strain-gage pressure transducers¹¹ housed in two sealed water-cooled containers mounted in the test cell.

The accuracy of the heat transfer measurements is estimated to be within $\pm 10\%$ for most of the measurements, and approximately $\pm 15\%$ near the regions of somewhat discontinuous slope in heat transfer distribution (i. e., transition region and sphere-cone junction) and near the stagnation region at the higher angles of attack. The accuracy of the pressure measurements is approximately $\pm 5\%$.

• PRESSURE AND THERMOCOUPLE INSTRUMENTATION

• PRESSURE INSTRUMENTATION ONLY

• WELLS

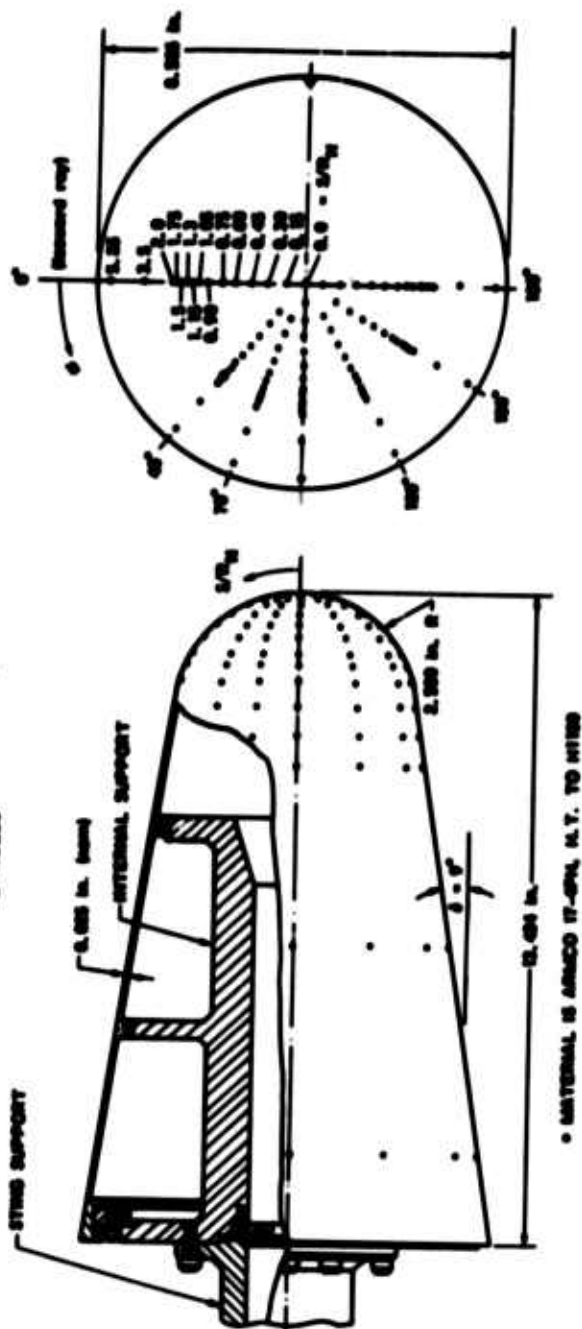


Figure 1. Schematic of Model and Instrumentation Locations

IV. EXPERIMENTAL RESULTS

Only representative data plots which depict the pertinent results determined in this study are included in this report. Tabulations of the data obtained at each of the test conditions are included in Appendix A. An overview of the data is presented in this section. Comparisons with various numerical calculations are presented and discussed in Section V.

Figure 2 shows the windward and leeward pressure distributions on the conical surface for the angles of attack considered in this test program. Included in this figure are the numerical results obtained using the angle-of-attack inviscid flow field computer code described in Ref. 12. Good agreement between the numerical calculations and the measured distributions is noted (except in regions where viscous-inviscid interactions should be important) for all angles of attack at which the calculations could be made.

Included in Fig. 3a-d are the corresponding plots of the heat transfer distributions on the conical surface for the four different freestream conditions at which tests were conducted. At the three higher freestream Reynolds number conditions, the flow undergoes transition and achieves the fully turbulent state on the hemisphere. However, at the $Re_{\infty} = 4.6(10)^6$ condition, the flow is laminar, becoming transitional/turbulent on the conical surface as the angle of attack is increased. It should be noted that, except in regions where the flow is transitional, the distributions of both the heat transfer and the pressure are similar. Also, as the angle of attack is increased, it is seen that the heat transfer on the leeward side decreases at a faster rate than it increases on the windward ray. It should be pointed out that the flow is transitional^{*} along the windward ray for $\alpha = 20, 25^\circ$ and 27.5° at the $Re_{\infty} = 11(10)^6$ freestream condition.

^{*}This becomes apparent when the distributions along the entire windward and neighboring rays at each angle of attack are plotted and compared.

Preceding page blank

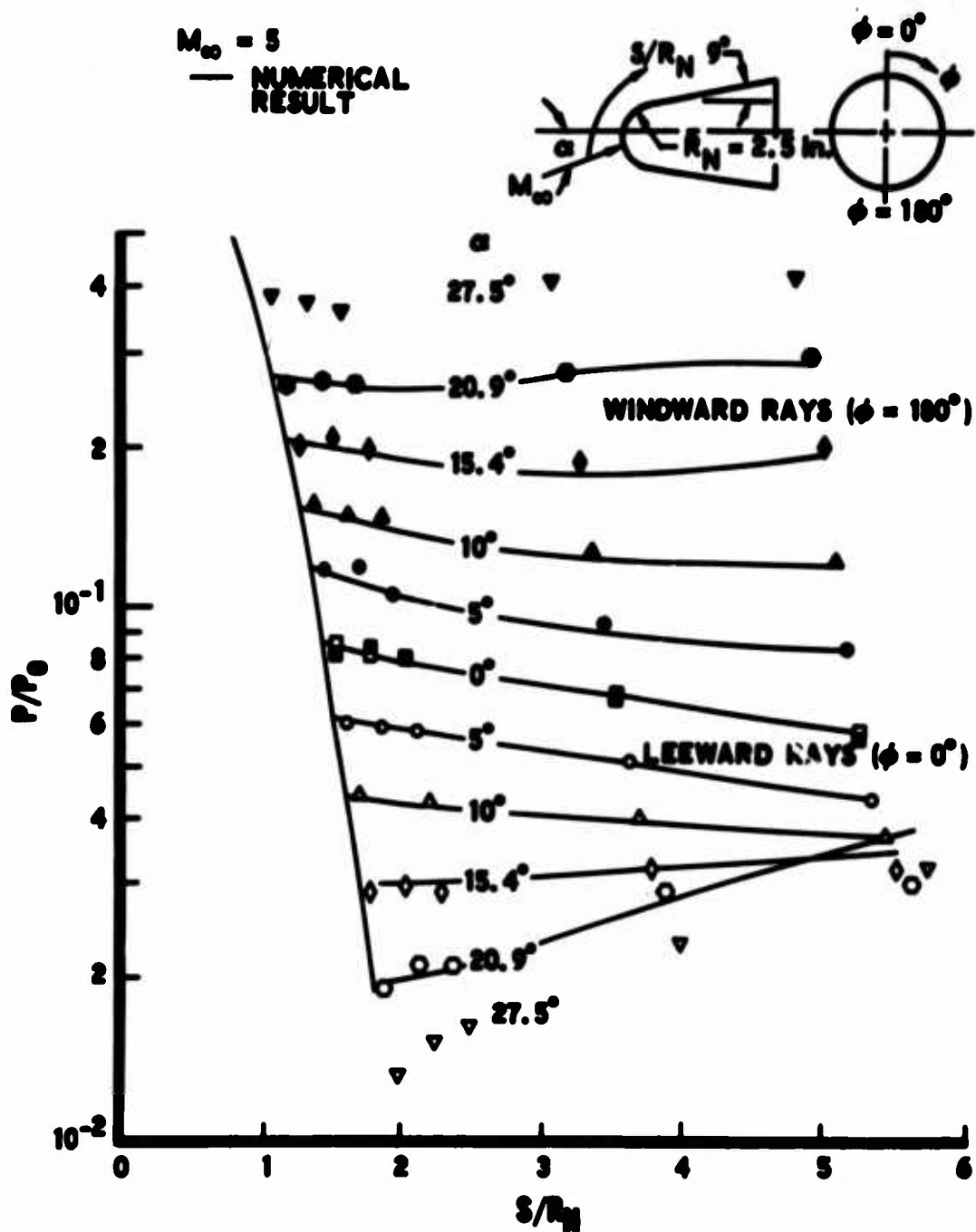


Fig. 2. Surface Pressure Distributions Along the Windward and Leeward Rays at Various Angles of Attack

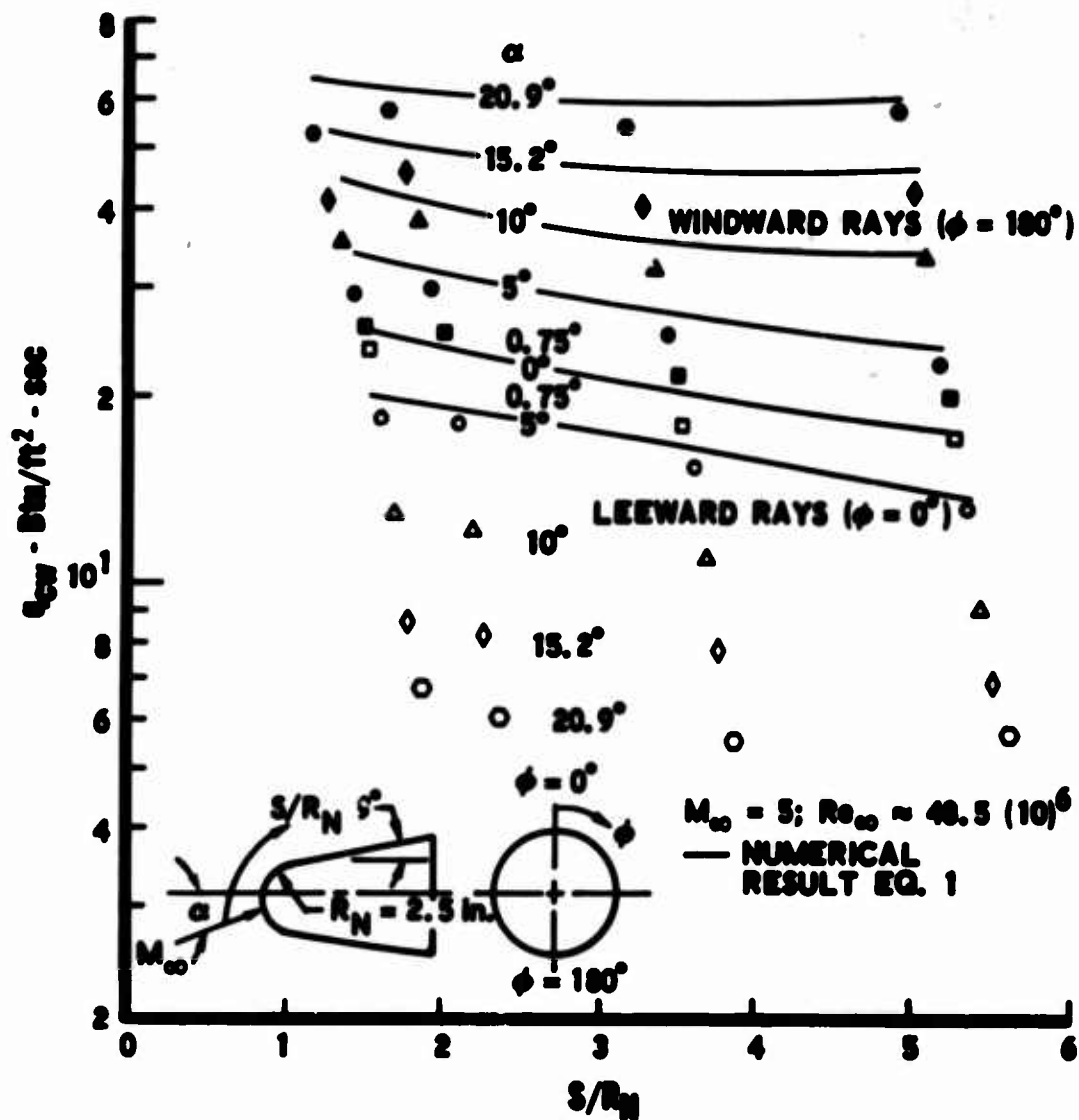


Fig. 3a

Figs. 3. Heat Transfer Distributions Along the Windward and Leeward Rays at Various Angles of Attack

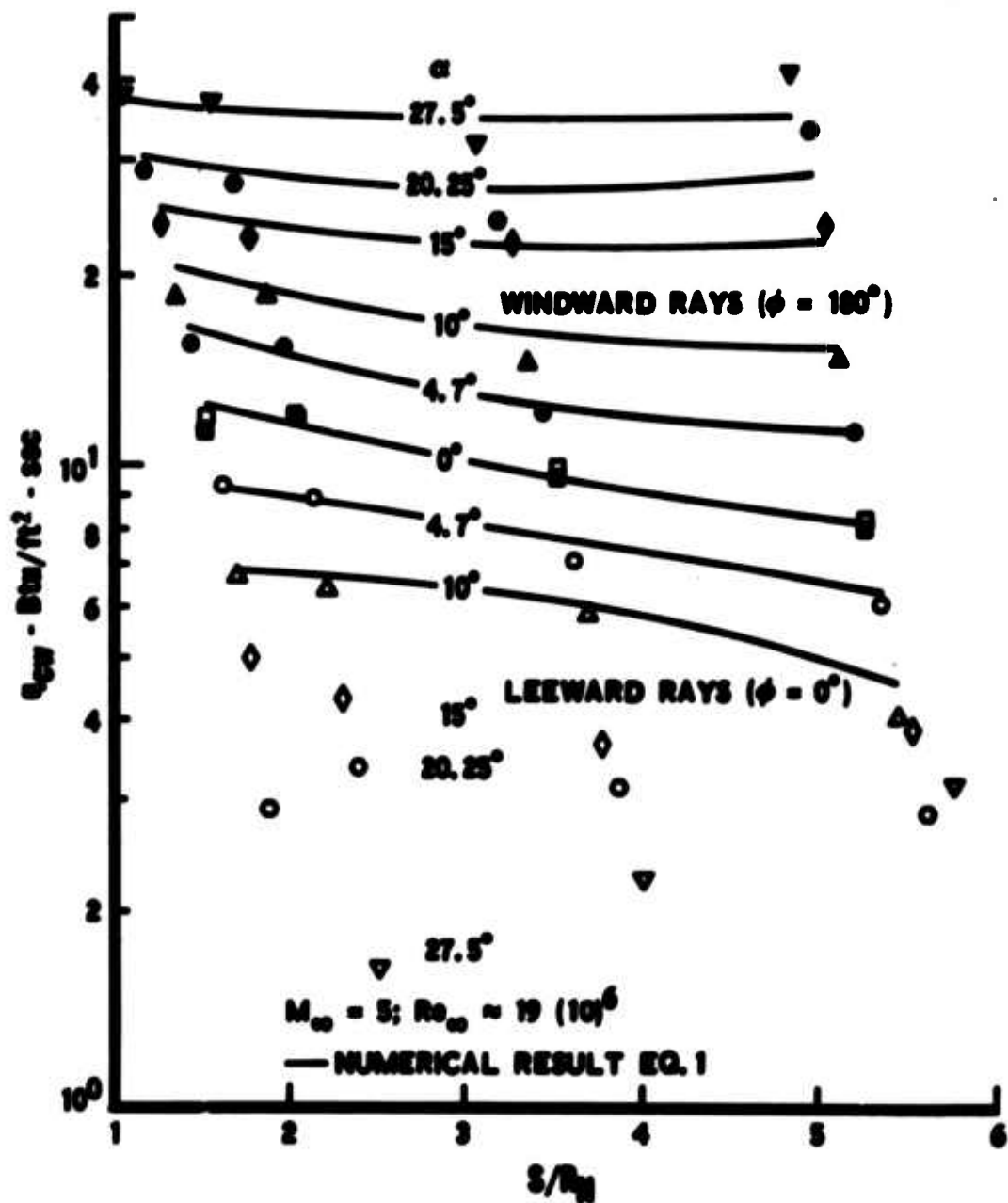


Fig. 3b

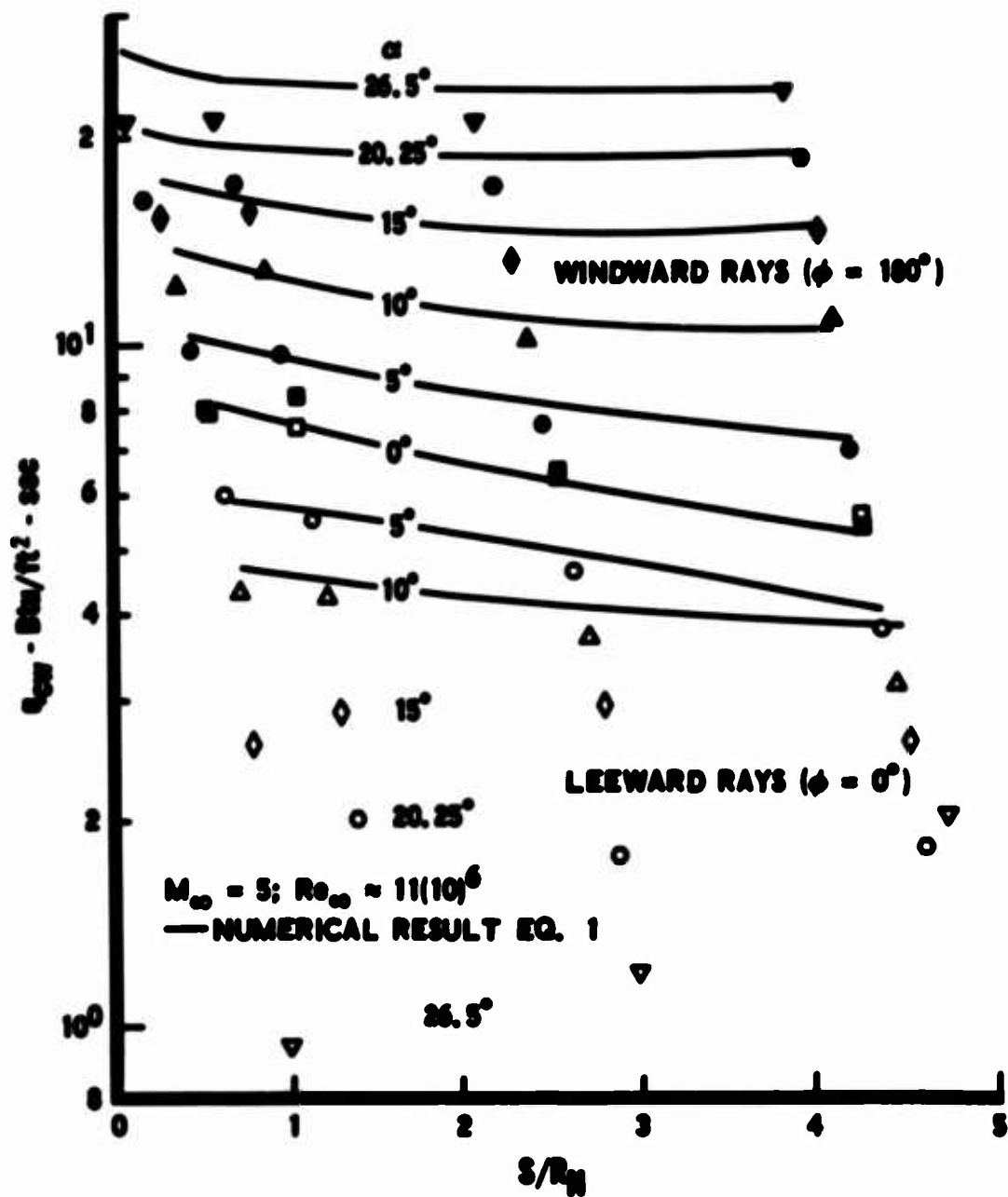


Fig. 3c

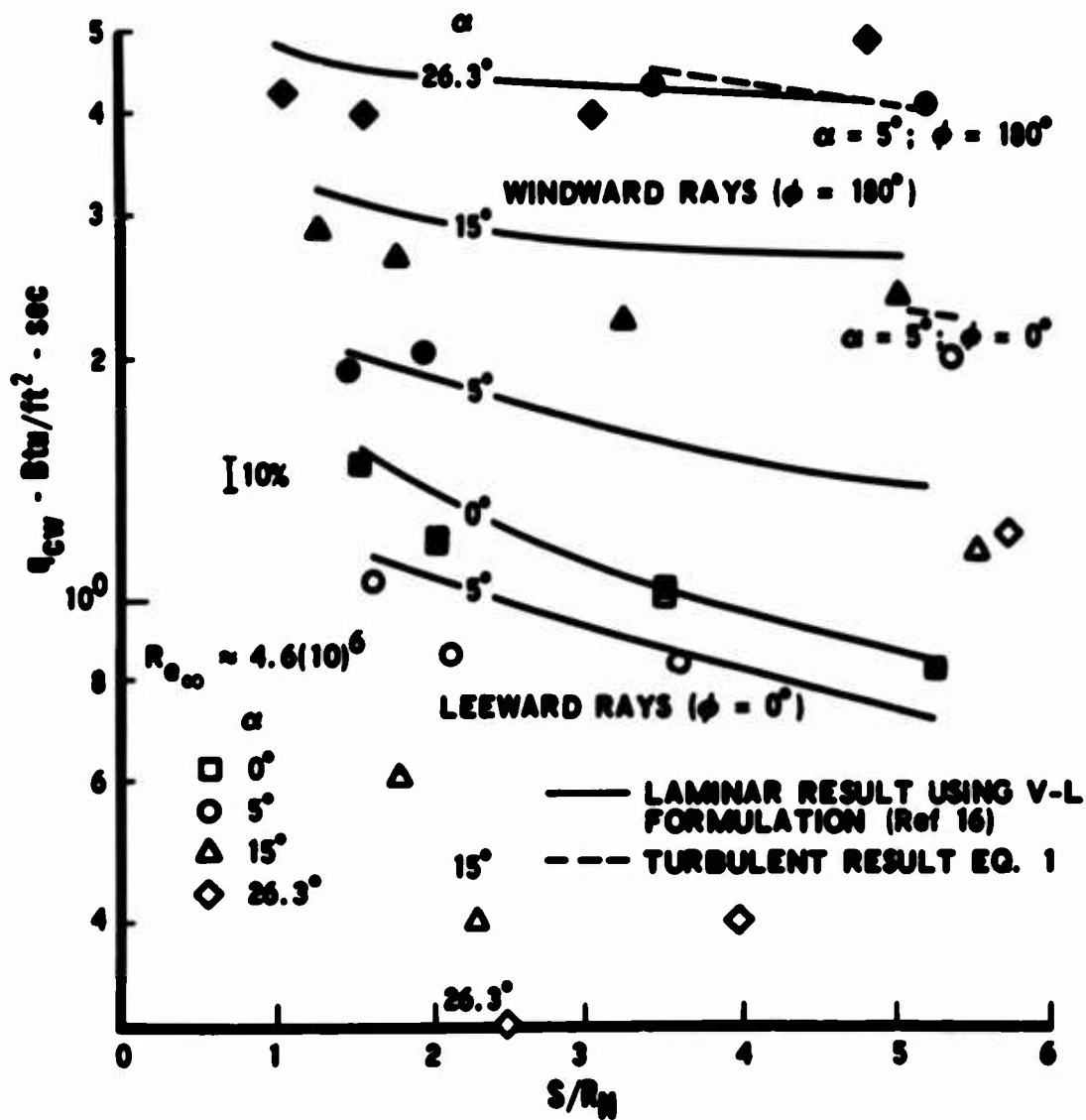


Fig. 3d

Figure 4a shows the nondimensional cold wall heat transfer (q_{cw}/q_{cw_0}) distribution on the hemispherical cap plotted with respect to the nondimensional streamline coordinate l/R_N . (All values of q_{cw_0} appearing in the paper are calculated values obtained using the Fay and Riddell¹³ relationship.) Here the data for each of the angles of attack considered at the $Re_\infty = 48.5(10)^6$ condition have been superimposed on one figure. This type of plot is convenient, since the angle-of-attack distributions on the hemisphere should be self-similar in this coordinate system. Indeed, within the stated experimental error, this is the case. At this freestream condition, the flow becomes transitional at approximately station $l/R_N = 0.2$ and achieves the fully turbulent state at approximately $l/R_N = 0.4$; thus, the peak heating point has been measured. The T_w/T_0 ratio varied between 0.24 to 0.27 for these tests and, to a small degree, some of the broadening of the transition region¹⁴ can be attributed to this variation. Similar plots for individual tests at Re_∞ values of $19(10)^6$ and $11(10)^6$ are shown in Figs. 4b and 4c. In these figures, each of the individual circumferential data points has been indicated, and the transition from the laminar to the turbulent state is clearly shown. It is also interesting to note (Figs. 3, 4) that the peak heating point is still on the hemisphere for angles of attack up to three times the cone half-angle.

The location of transition point at each of these freestream conditions [$Re_\infty = 48.5, 19, \text{ and } 11(10)^6$] was determined by plotting the heat transfer distributions on a log-log scale and determining the intersection of two straight lines drawn through the laminar and transitional data.¹⁵ The transition points were also determined by matching the distributions with a numerically calculated heat transfer distribution of the type discussed in the next section. Each of these methods is subject to error, but is accurate enough to allow for a relatively accurate determination of the transition point. This, in part, results from the fact that the transition zone at hypersonic conditions is narrow; thus, the number of data points located in the zone for this particular instrumentation layout is not large. Also, it was found that, at the higher angles of attack, the transition point on the two most windward rays was usually further away from the stagnation region than on the other rays.

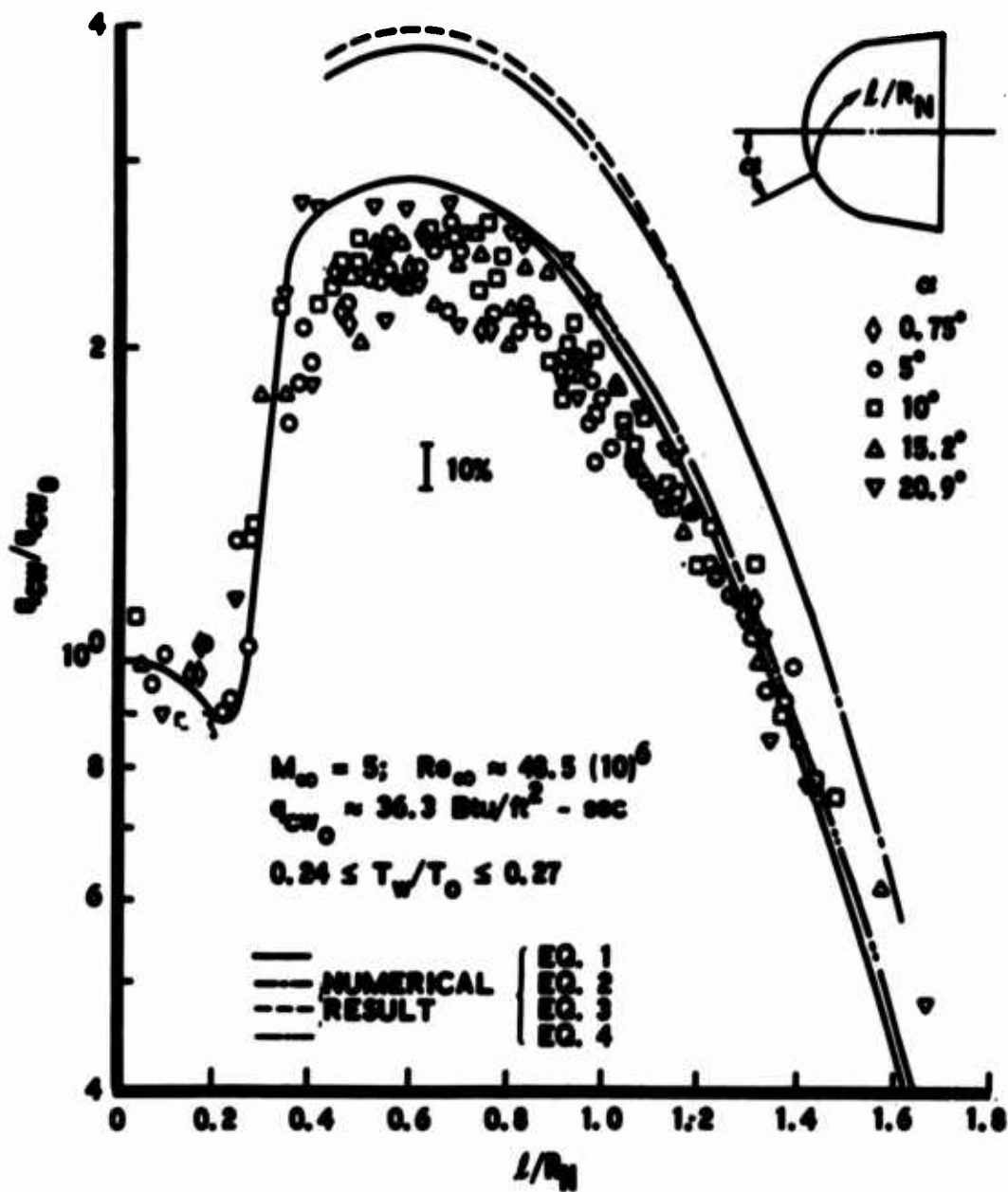


Fig. 4a

Figs. 4. Heat Transfer Distribution on the Hemispherical Cap

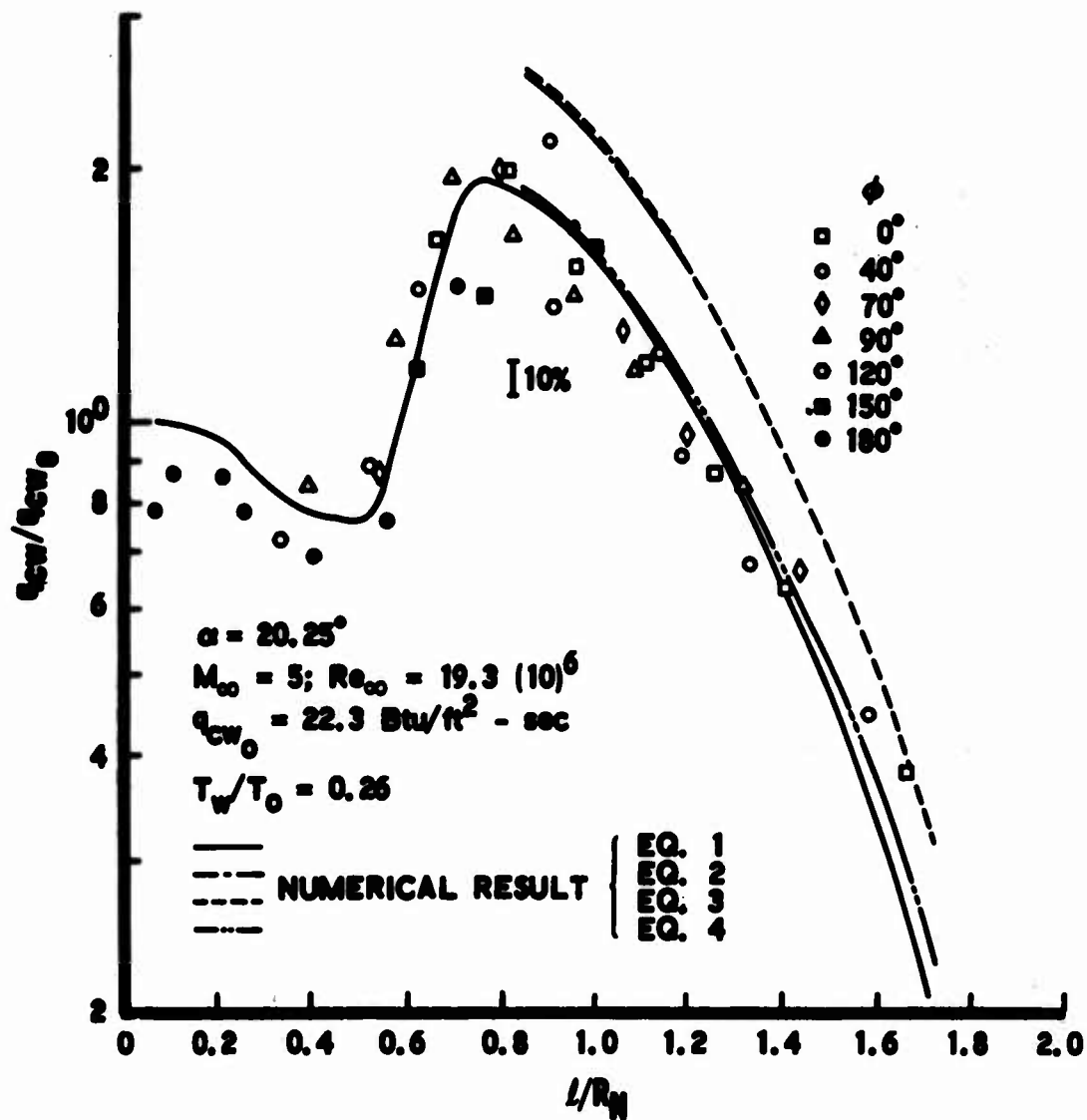


Fig. 4b

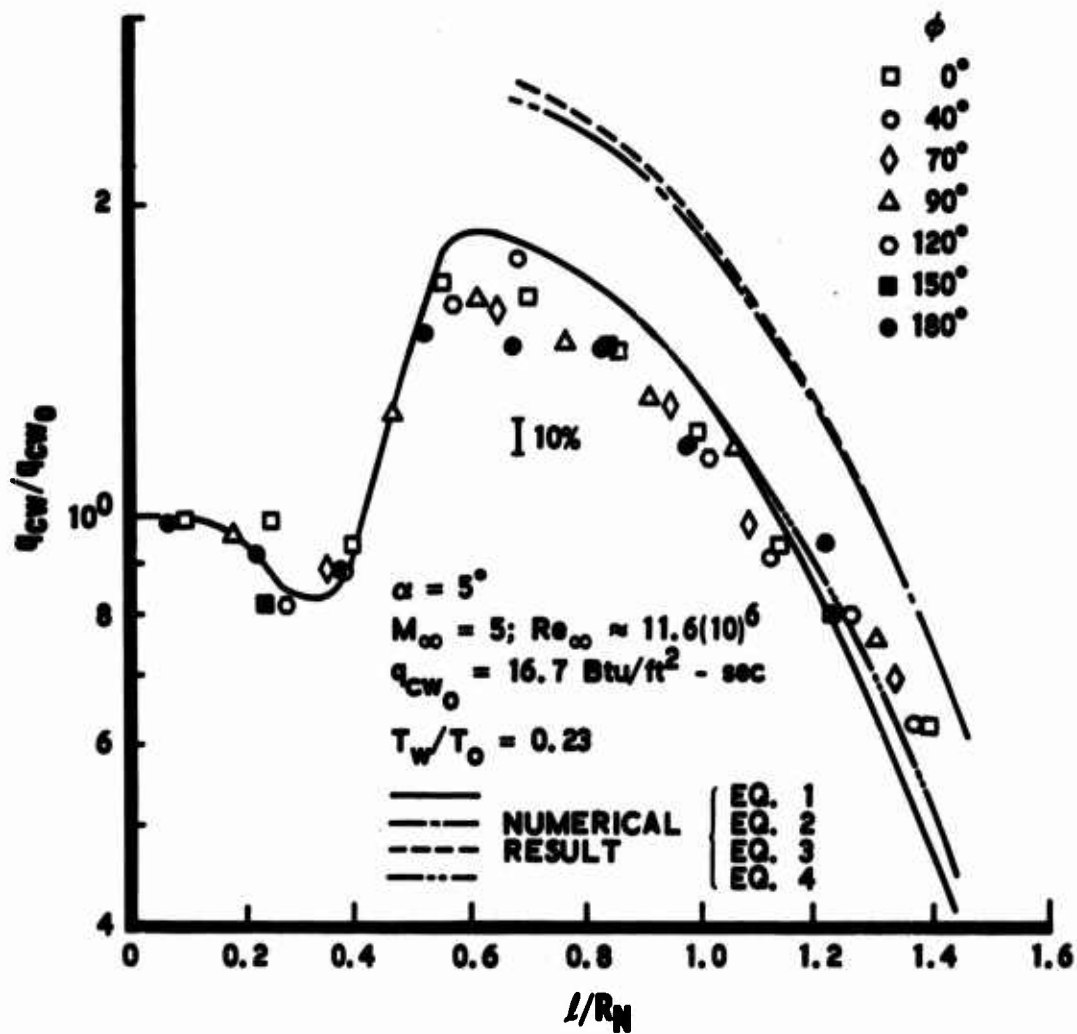


Fig. 4c

Since the flow on the hemisphere is self-similar with respect to the stream-line coordinate, this should not be the case when transition occurs on the hemisphere. This result is probably associated with the injection of the model into the test section and with the fact that the windward ray is the last to enter the test core. The second method is subject to the validity and accuracy of the heat transfer formulations used to determine the numerical distribution.

The results obtained for a few runs at the $Re_\infty = 48.5$ and $19(10)^6$ conditions are shown in Fig. 5. The results obtained by the two methods discussed previously are indicated by the designations Method 1 and 2, respectively. Included in this figure are various transition data obtained on smooth blunt nosetips, which were originally compiled in Ref. 16. Here, the value of Re_{θ_T} at the transition point has been plotted against the corresponding edge Mach number. Each of the test conditions is indicated in the legend of the figure, and the variation in the T_w/T_o ratio should be noted. The present variables (Re_{θ_T} and Me_T) certainly cannot adequately represent the variation of the transition location with all the pertinent flow variables which affect the transition process, but it is evident from this figure that natural transition was achieved at these two test conditions. Similar results obtained for the $Re_\infty = 11(10)^6$ condition indicate that the boundary layer was prematurely tripped by some surface roughness which probably resulted from particle impacts. This occurred even though the model was hand polished between runs.

When the heat transfer ratio along any ray (or rather for any specific point on the surface) was plotted on a semilog scale as a function of angle of attack, the variation was found to be approximated very well by a straight line. This was the case as long as the flow was fully turbulent and not separated. Examples of this are shown in Figs. 6a-c for specific locations on the windward and leeward rays at each of the freestream conditions. This behavior was also observed in Ref. 1 and simplifies interpolations of the data to any inclusive angle of attack. As was found in Ref. 1, the yaw plane ($\phi = 90^\circ$) heat transfer rate on the conical surface is a very weak function of angle of attack. An example of this can be seen in Fig. 7, where the variation

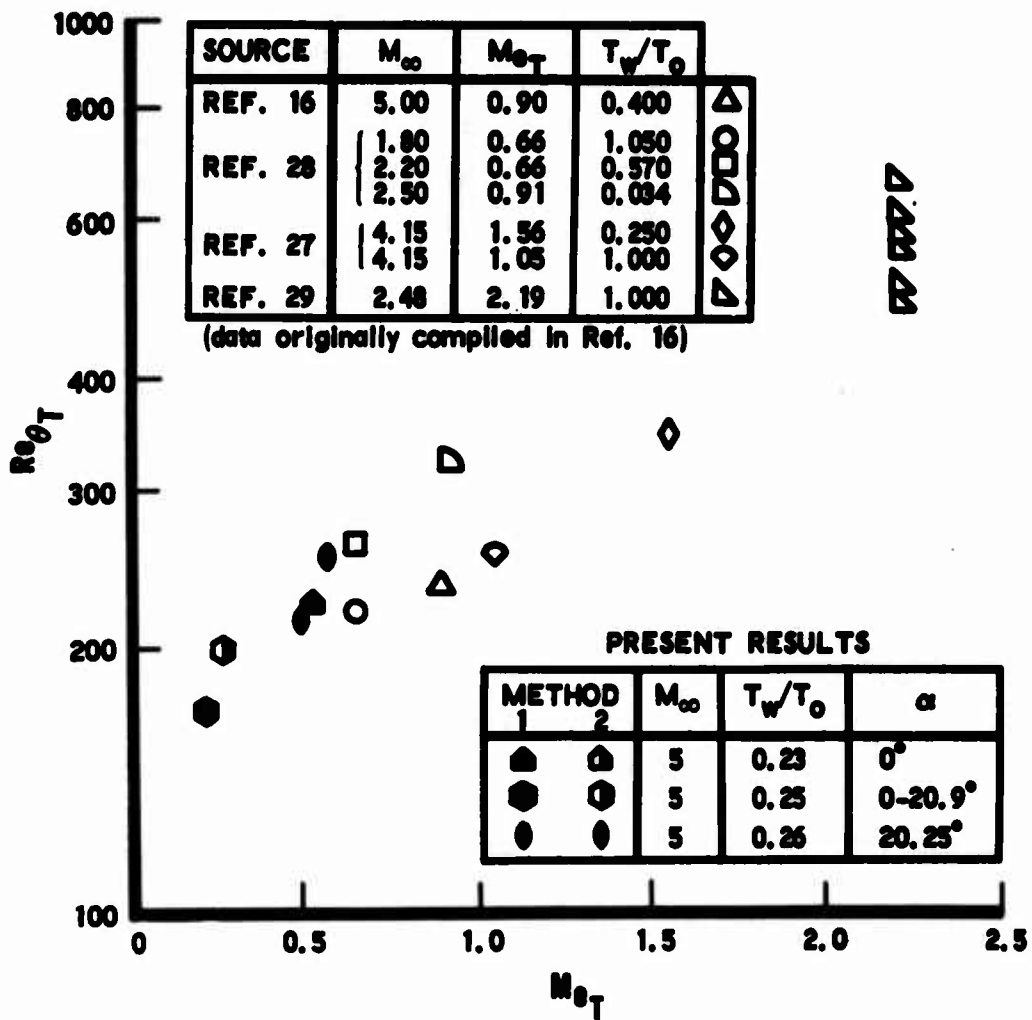


Fig. 5. Smooth Wall Transition Data on Blunt Nosetips

$M_\infty = 5$
 $Re_\infty \approx 40.5 (10)^6$
 — DATA FAIRING

S/R_N
 □ 1.05
 ○ 1.3
 △ 1.5
 ◇ 2.0
 ● 3.5
 ▼ 5.25

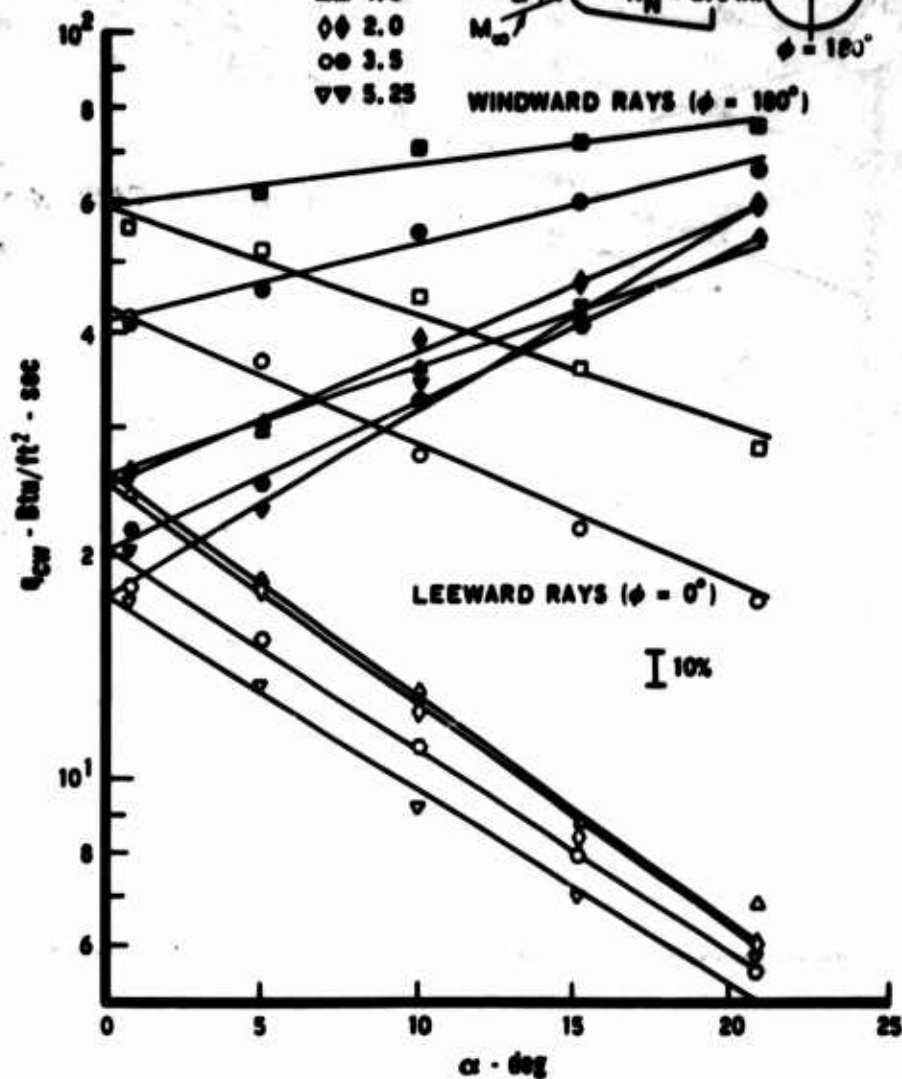
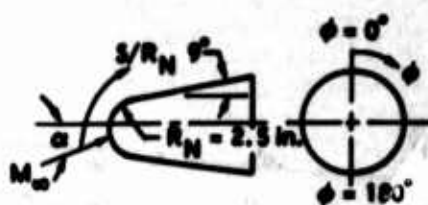


Fig. 6a

Figs. 6. Heat Transfer Variation with Angle of Attack at Various Stations Along the Windward and Leeward Rays

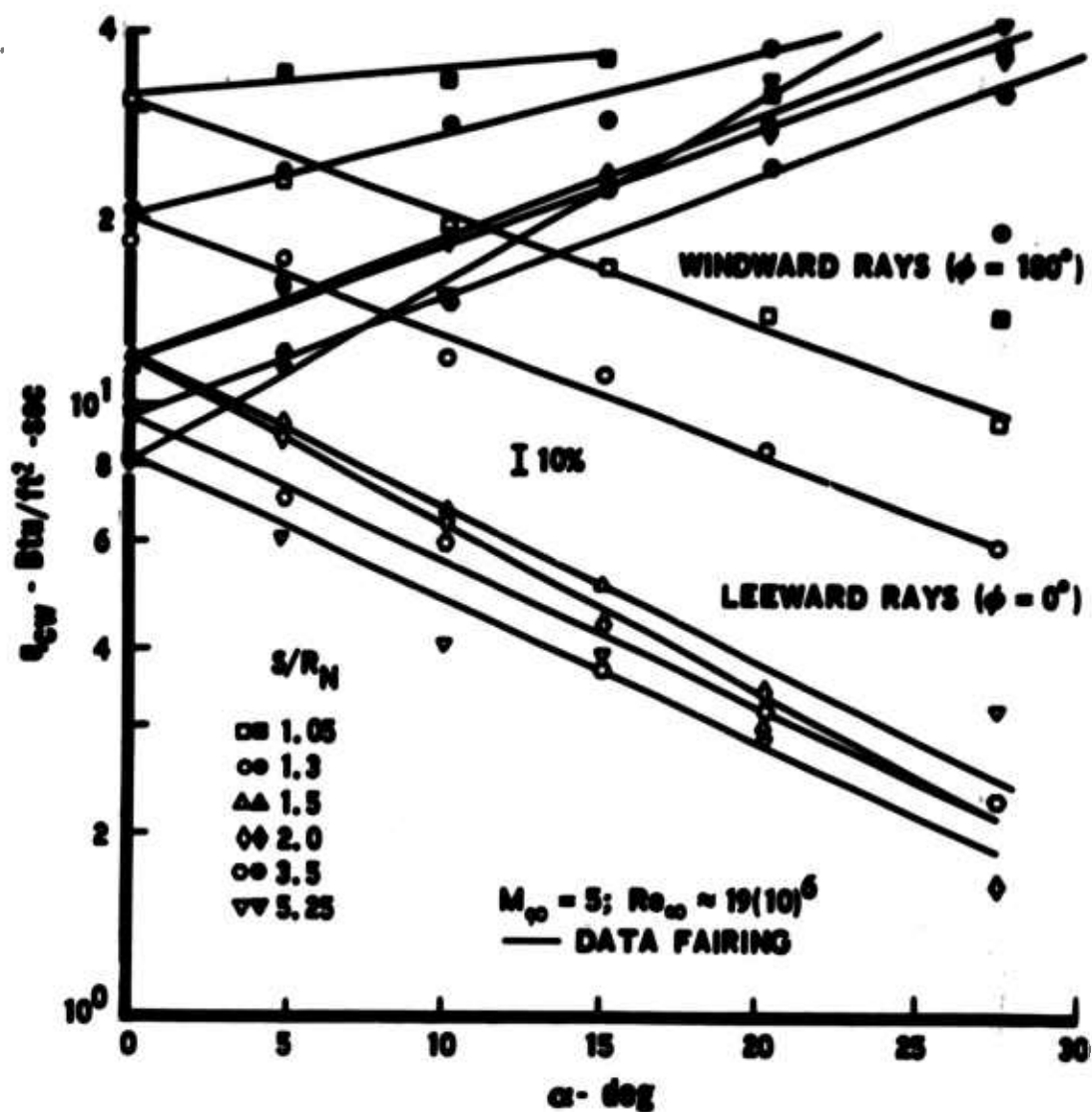


Fig. 6b

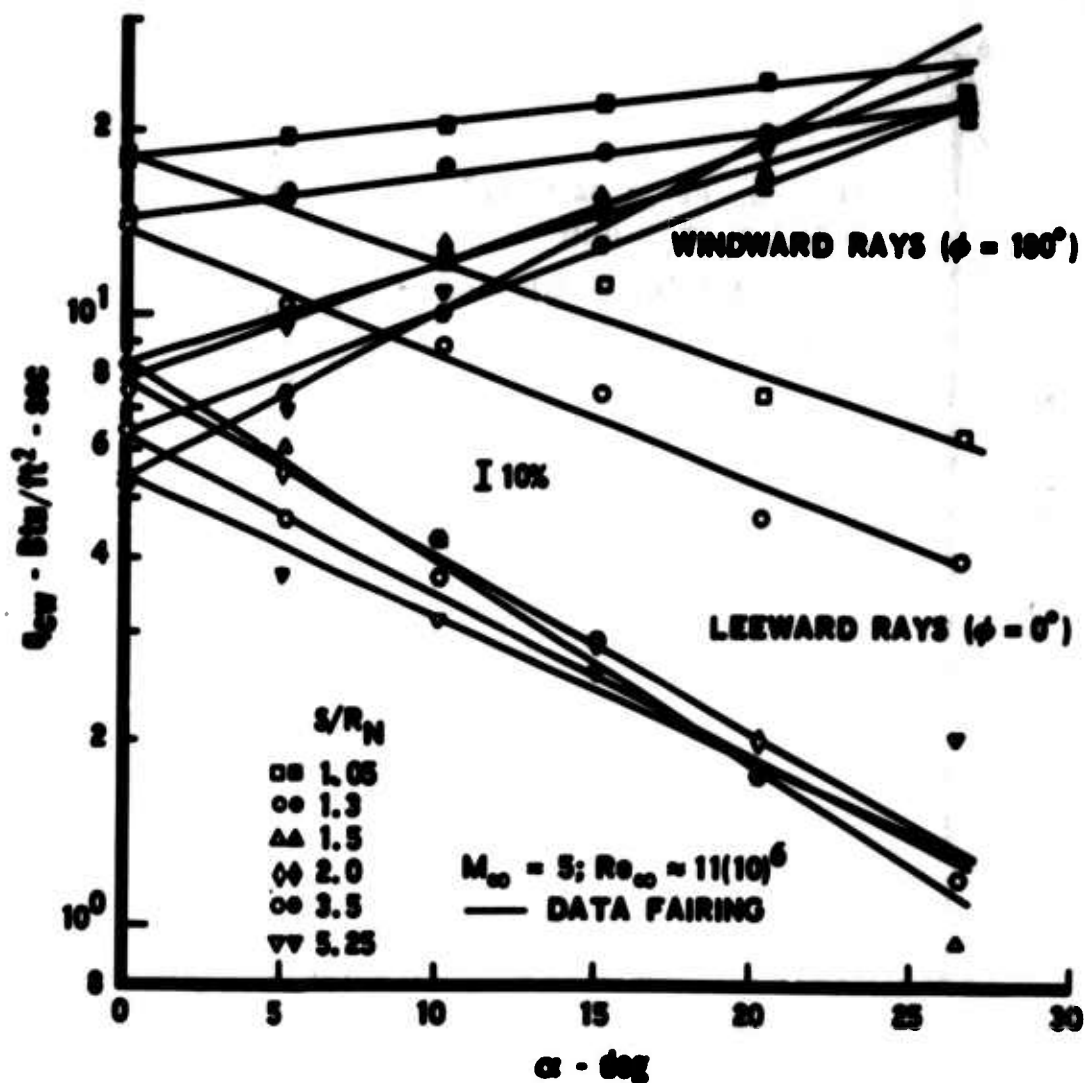


Fig. 6c

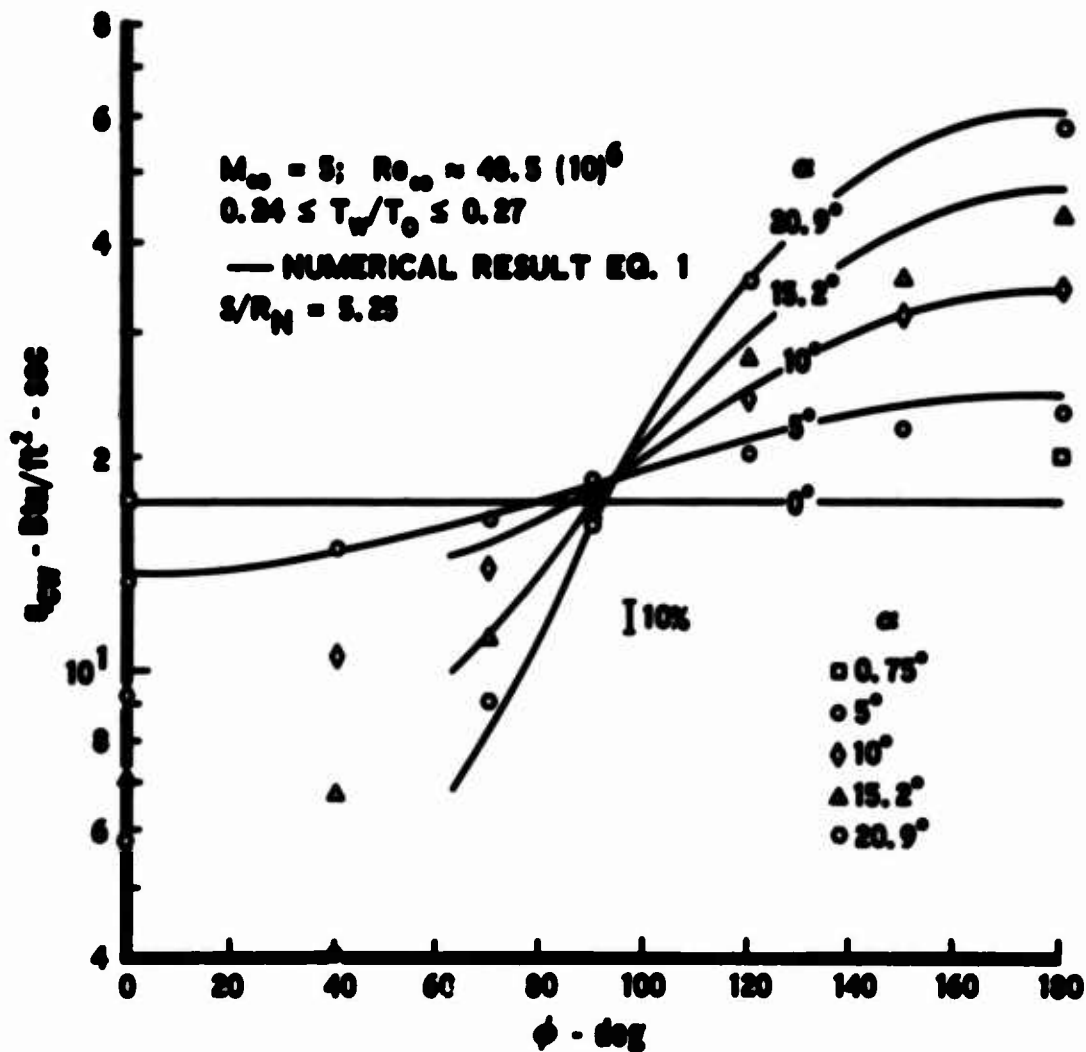


Fig. 7. Comparison Between Experimental and Calculated Circumferential Turbulent Heat Transfer Distributions at Station $S/R_N = 5.25$ for Various Angles of Attack

of the circumferential turbulent heat transfer distribution with angle of attack, at station $S/R_N = 5.25$, is shown for the $Re_\infty = 48.5(10)^6$ freestream condition.

The variation of the circumferential heat transfer distribution for various axial surface locations, measured with respect to the model centerline, is shown in Fig. 8. This type of planar section is interesting since it shows the circumferential variation in the geometric plane. In general, once the flow has become fully turbulent, the circumferential variation can be described by a cosine type variation. However, the distributions in the transitional regime become varied indeed, since at angle of attack the windward transition point moves rearward, with respect to a coordinate system centered at the $\alpha = 0^\circ$ stagnation point, while the leeward transition point moves forward. The subsequent effect of this type of heating distribution on nosetip ablation and the resulting shape change can be visualized.

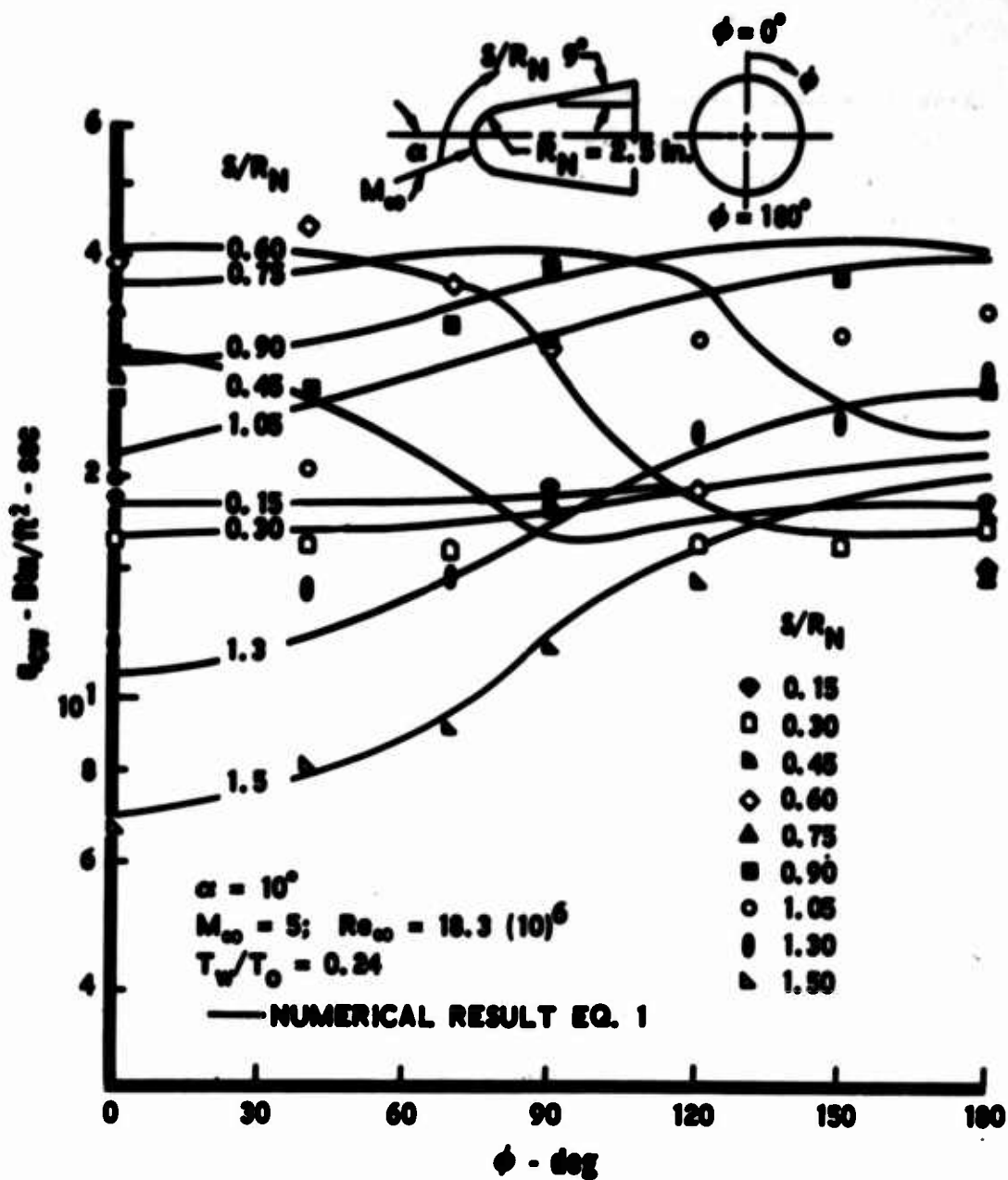


Fig. 8. Circumferential Variation of the Heat Transfer at Various Stations on the Hemisphere

V. COMPARISON WITH NUMERICAL RESULTS

Heat transfer rates computed along inviscid surface streamlines traced over the surface of the blunt cone at each angle of attack were compared to the data. The Fay and Riddell relation¹³ was used to calculate the stagnation heat flux, and Vaglio-Laurin's laminar relation¹⁷ was used to obtain the laminar heat transfer distribution. Four separate formulations were used to calculate the fully turbulent heat transfer rate, while the method of Ref. 18 was applied to the angle-of-attack case and used to determine the distribution in the transitional regime. The four methods are those proposed by Vaglio-Laurin,¹⁹ McCuen, et al.,²⁰ Walker,²¹ and DeJarnette and Tai.²² These formulations are given below, in their respective order.

$$q_w = A(H_{se} - H_w) \rho_e U_e h_2^{1/4} \mu_e \mu_{se}^{-3/5} \left\{ \int_0^l \rho_e U_e h_2^{5/4} dl \right\}^{-1/5} \quad (1)$$

$$q_w = A(H_r - H_w)^{5/4} \rho_1 U_e (h_2 \mu_1)^{1/4} \left\{ \int_0^l \rho_1 U_e \mu_1^{1/4} [h_2 (H_r - H_w)]^{5/4} dl \right\}^{-1/5} \quad (2)$$

$$q_w = A[(H_r - H_w)\epsilon]^{5/4} \rho_e U_e (\mu_e h_2)^{1/4} \left\{ \int_0^l \rho_e U_e \mu_e^{1/4} \times [(H_r - H_w) h_2 \epsilon]^{5/4} dl \right\}^{-1/5} \quad (3)$$

$$q_w = A(H_{ee} - H_w) \rho_e^{1.05} U_e^{1/4} h_2^{4/5} \mu_e^{1/20} \nu_e^{-3/5} \times \left\{ \int_0^1 \rho_e^{5/4} U_e^{1/4} h_2^{5/4} d\ell \right\}^{-1/5} \quad (4)$$

where

$$A = 0.0296 P_r^{-2/3}$$

$$c = (\mu_3/\mu_e)^{1/5} (\rho_3/\rho_e)^{4/5} \quad (5a)$$

and

$$h_1 = 0.36 h_e + 0.19 H_r + 0.45 H_w$$

$$h_3 = (0.5 - 0.22 P_r^{1/3}) h_e + 0.22 P_r^{1/3} H_{se} + 0.5 H_w$$

$$h_4 = 0.5 h_e + 0.5 H_w + 0.22 P_r^{1/3} \frac{\gamma-1}{2} M_e^2 h_e \quad (5b)$$

Equations (5b) define the reference enthalpy which is used together with the pressure to define the reference conditions ρ_1 , μ_1 , ρ_3 , μ_3 , and ν_4 used in Eqs. (2) through (4).

Substitution of Eq. (5a) into Eq. (3) demonstrates that Eqs. (2) and (3) are of exactly the same form, except that the definitions of their respective reference conditions (Eqs. 5b) are slightly different. Similarly, a comparison of Eqs. (1) and (4) will show that Eq. (4) is only slightly different than Eq. (1).

The major difference between the two groups* (Eqs. 1 and 4 and Eqs. 2 and 3) is the use of edge and/or reference conditions to define the

* Equation (4) is very weakly dependent on reference conditions and is very similar to Eq. (1) in functional form. Also, the subsequent heat transfer rates calculated for these test conditions agree within a few percent with those obtained using Eq. (1). Thus, they have been grouped for convenience.

local heat transfer rate. In general, the heat transfer level predicted by these two groups is different, with the disagreement increasing as the T_w/T_o ratio decreases. In this regard, the data obtained from this test program are especially suited to determine which is the better approximation at moderately cold wall conditions.

The streamline patterns were determined using the experimental pressure distributions and were computed from the most forward point on the model to the most rearward station. The streamlines on the hemisphere were traced along great circles emanating from the most forward point on the model, while the streamlines on the conical surface were traced using the technique described in Refs. 1, 23, and 24. The effect of streamline spreading was included in all of these calculations. Perfect gas properties were used and entropy swallowing was neglected. This latter approximation is a good assumption over most of the range of conditions examined herein, except at the higher angles of attack on the leeward side.¹ It must be emphasized that the identical freestream conditions, surface pressure distributions, edge conditions, viscosity relation (Sutherland model) and Prandtl number ($P_r = 0.716$) were used in Eqs. (1)-(5) in evaluating the heat transfer at a specific test condition. Thus, any variation in the subsequent heat transfer rate for a given test is only due to the model itself. Each relation (Eqs. 1-4) was appropriately modified ($H_{r, se} - H_w = H_{se}$) to yield the corresponding cold wall heat transfer rate so that the numerical results could be directly compared to the data.

Figures 4a-c show the results of some of these comparisons. In general, the results obtained using Eqs. (2)-(4) are shown downstream of the point where the fully turbulent rate has been achieved. However, for the Vaglio-Laurin formulation (Eq. 1), the theory of Ref. 18 has been applied to describe the transition from the laminar to the turbulent state. Here it is noticed that the Vaglio-Laurin distribution agrees, within the experimental error, with the data for each of the freestream conditions tested. In all cases, Eq. (4) yielded essentially (always a few percent higher) the same

distribution as Eq. (1) and therefore was not included where it would degrade the clarity of the respective figure. For each test condition, Eqs. (2) and (3) overpredict the heat transfer rate over the entire hemisphere. Equations (2) and (3) yield essentially the same results for these test conditions, except for the effect of the different reference enthalpy formulation near the peak heating point; thus, only one numerically determined curve is shown in most figures. The distribution in the transitional regime is adequately predicted by the theory of Ref. 18, although more comprehensive statements cannot be made without a more detailed determination of the heat transfer distribution in this region.

Figure 9 shows the heat transfer rate distribution for the zero angle-of-attack case at the $Re_{\phi} = 19(10)^6$ test condition. It should be pointed out that for this particular case the neglect of entropy swallowing effects is a very good approximation, since only the first five nose radii are being considered. Included in this figure is a numerical result* obtained using the finite difference turbulent boundary layer program described in Ref. 25. The identical pressure distribution and edge conditions were used in this calculation. This boundary layer program uses an eddy viscosity model which accounts for pressure gradient effects. The resulting distribution on the hemisphere falls between the other results, and overpredicts the level on the conical surface. Equation (1) shows good agreement with the data, while Eqs. (2) and (3) substantially overpredict the data over the entire surface. This trend was found to hold for all the measured distributions at each angle of attack. Examples of this trend along the conical surface are shown in Figs. 10a-b, where the longitudinal distributions along various rays are shown for two angles of attack, $\alpha = 15^\circ$ and $\alpha = 20.25^\circ$. Here it is noticed that the distributions computed using Eq. (1) show good agreement with the data, while the corresponding rates obtained using Eqs. (2) and (3) do not. Only the $\phi = 180^\circ$ and 90° solutions obtained using Eqs. (2) and (3)

*This result was graciously supplied by N. Jaffe of The Aerospace Corp.

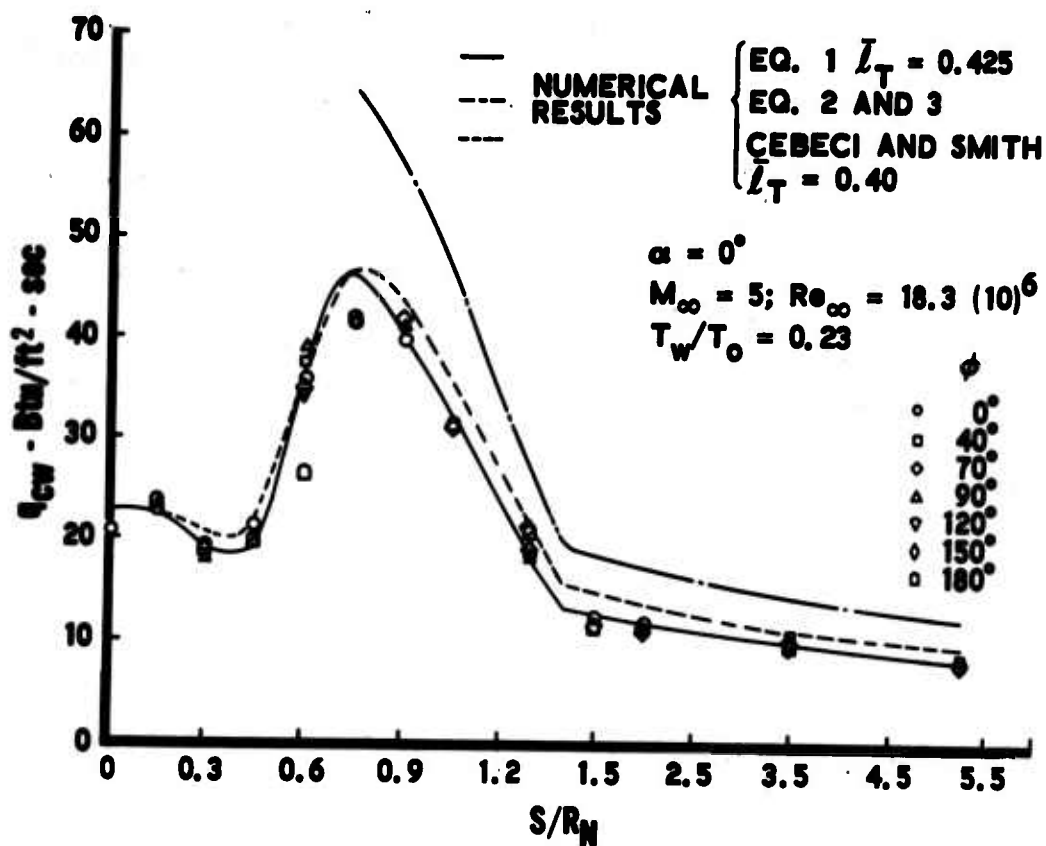


Fig. 9. Comparison Between the Experimental and Calculated Heat Transfer Distributions at $\alpha = 10^\circ$; $Re_\infty = 18.3(10)^6$

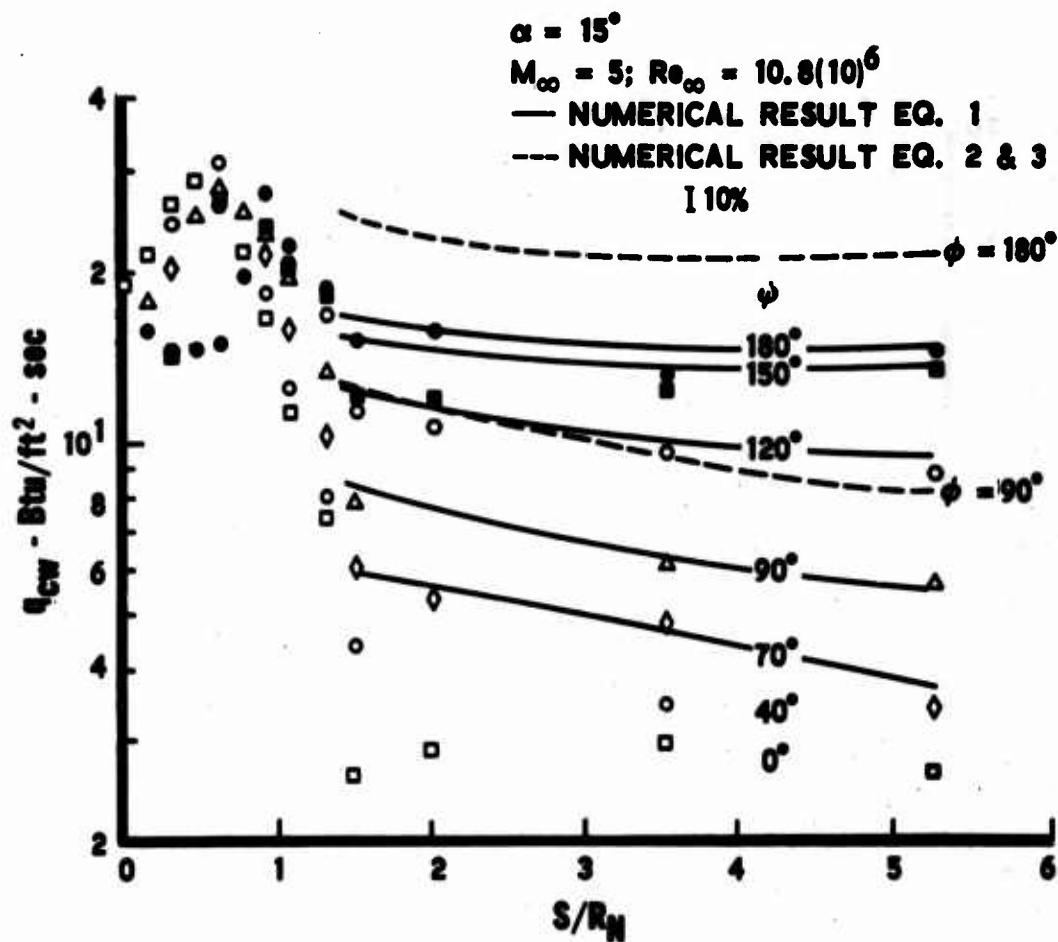


Fig. 10a

Figs. 10. Comparison Between the Experimental and Calculated Circumferential Pressure Distributions on the Conical Surface

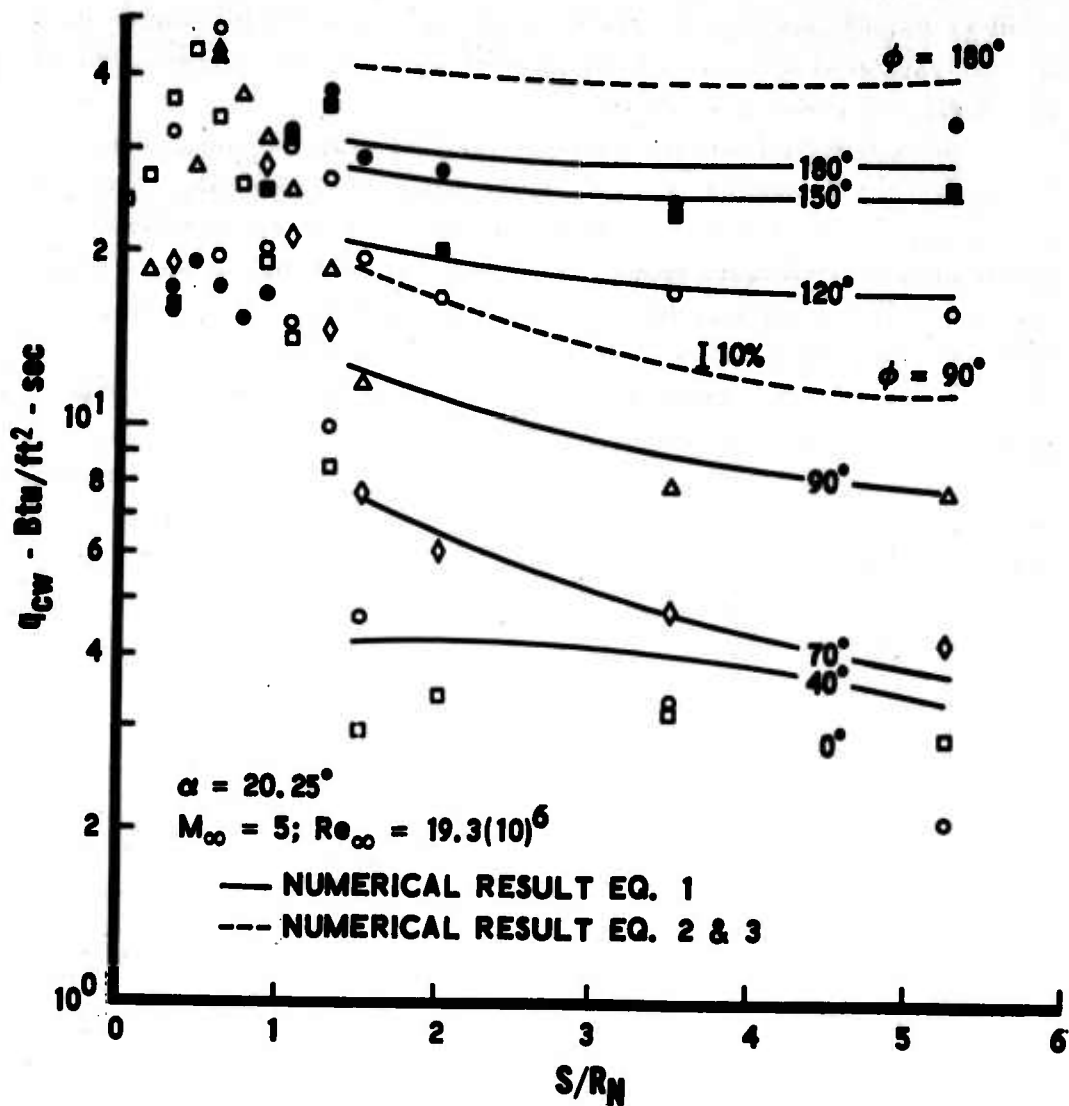
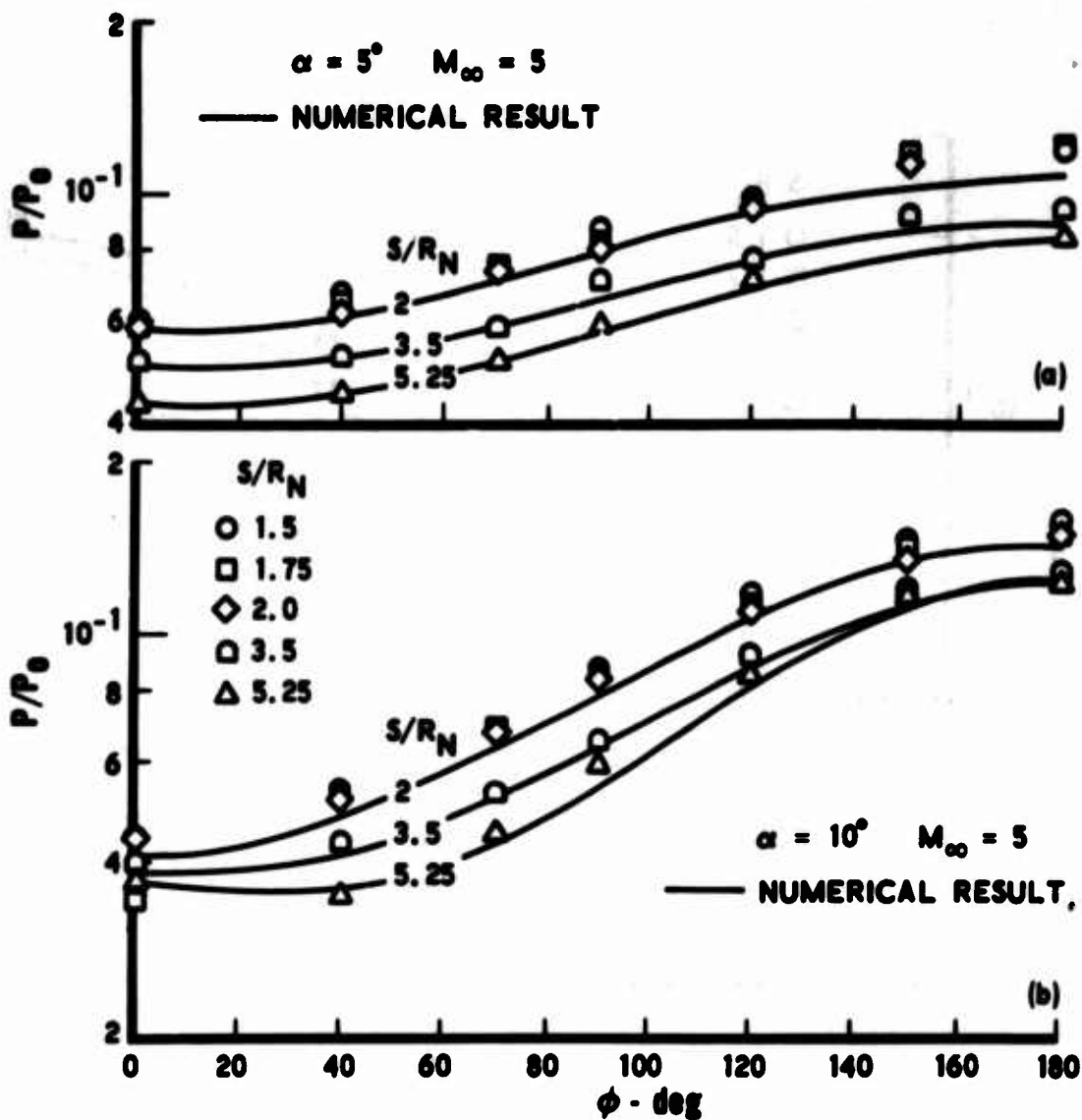


Fig. 10b

have been presented in these figures in order to clarify the presentation. Further comparisons between the experimental data and the numerical results obtained using Eq. (1) are shown in Figs. 3a-c for the windward and leeward rays at various angles of attack for each freestream test condition. In general, the agreement is good.

The comparison between the numerical and experimental circumferential heat transfer distributions on the hemisphere using Eq. (1) and the transitional theory of Ref. 18 is shown in Fig. 8. The agreement in both magnitude and distribution is good, even in the transitional regime. The calculated circumferential distributions at station $S/R_N = 5.25$ were compared with the data for each of the angles of attack, and the results are shown in Fig. 7. The agreement between the numerical results and the measured distributions is good for all the angles of attack, except on the leeward side at the higher angles of attack. In this region, entropy swallowing should become important¹; thus, agreement in this region would not be expected. Also, at the higher angles of attack, separation has occurred on portions of the leeward side, so that the approach used herein is invalid in those regions. An indication of the location of the separation region can be obtained from the circumferential pressure plots included in Figs. 11a-e. In these figures, the circumferential surface pressure distributions calculated using the inviscid computer code described in Ref. 12 are compared to the corresponding measured distributions. Good agreement is noted, except in regions where viscous-inviscid interactions are important.

The pressure distribution on the hemispherical sections is shown in Fig. 12. Here the pressure data measured at $\alpha = 20.9^\circ$ has been plotted with respect to the streamline coordinate \bar{r} and is seen to collapse to the proper self-similar curve. The numerical result obtained using the inviscid computer code described in Ref. 12 is included in this figure along with the distribution calculated using the modified Newtonian theory.



Figs. 11a-b

Figs. 11. Comparison Between the Experimental and Calculated Circumferential Pressure Distributions on the Conical Surface

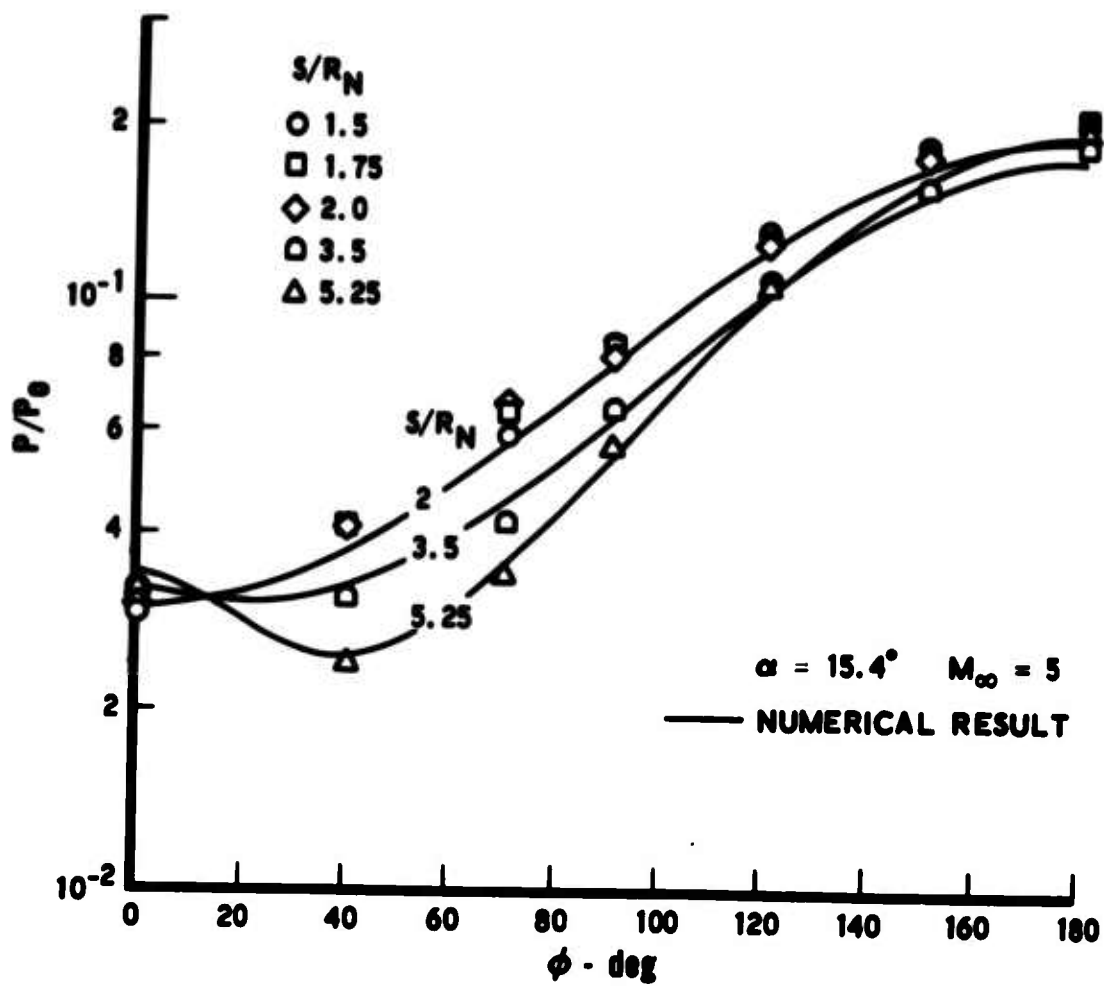


Fig. 11c

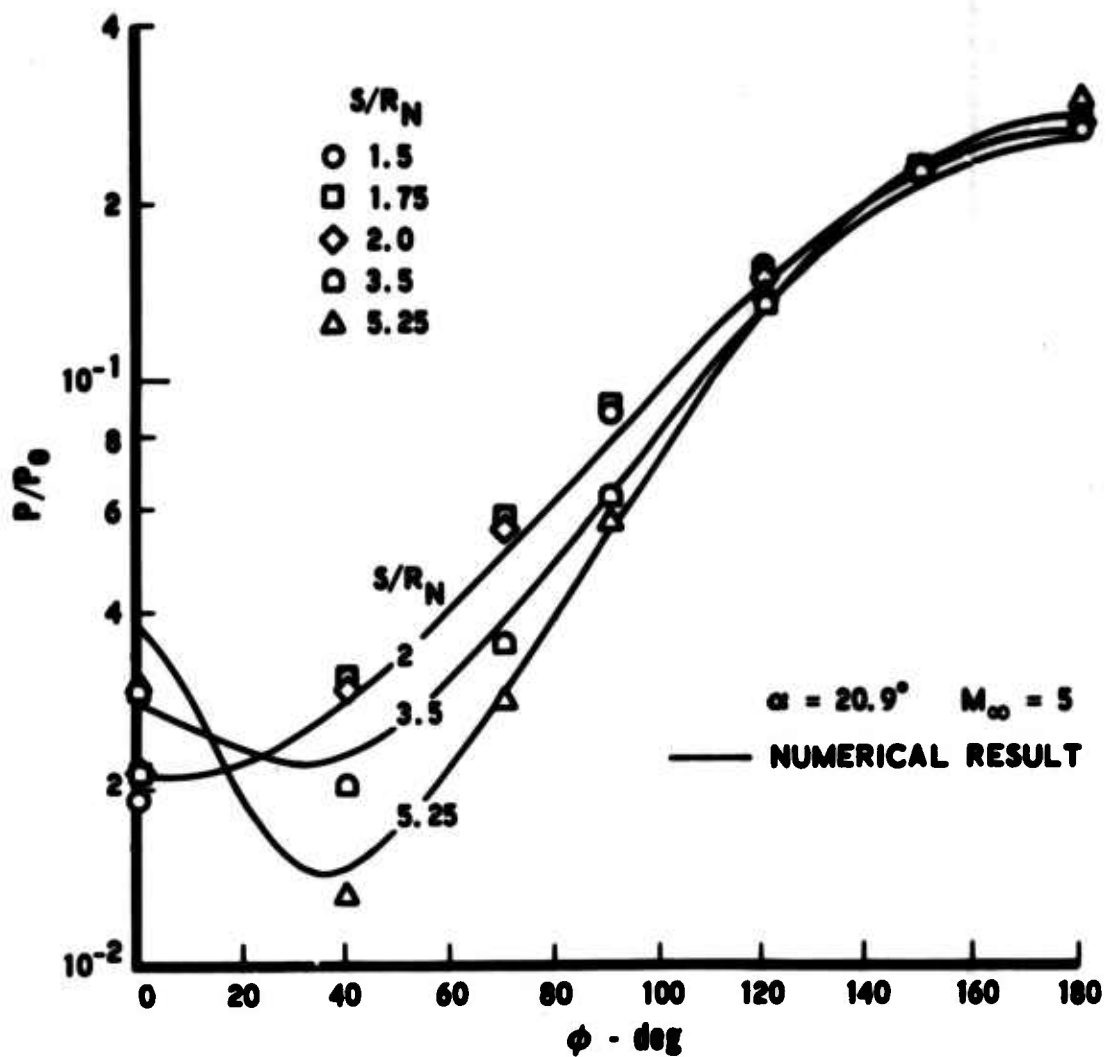


Fig. 11d

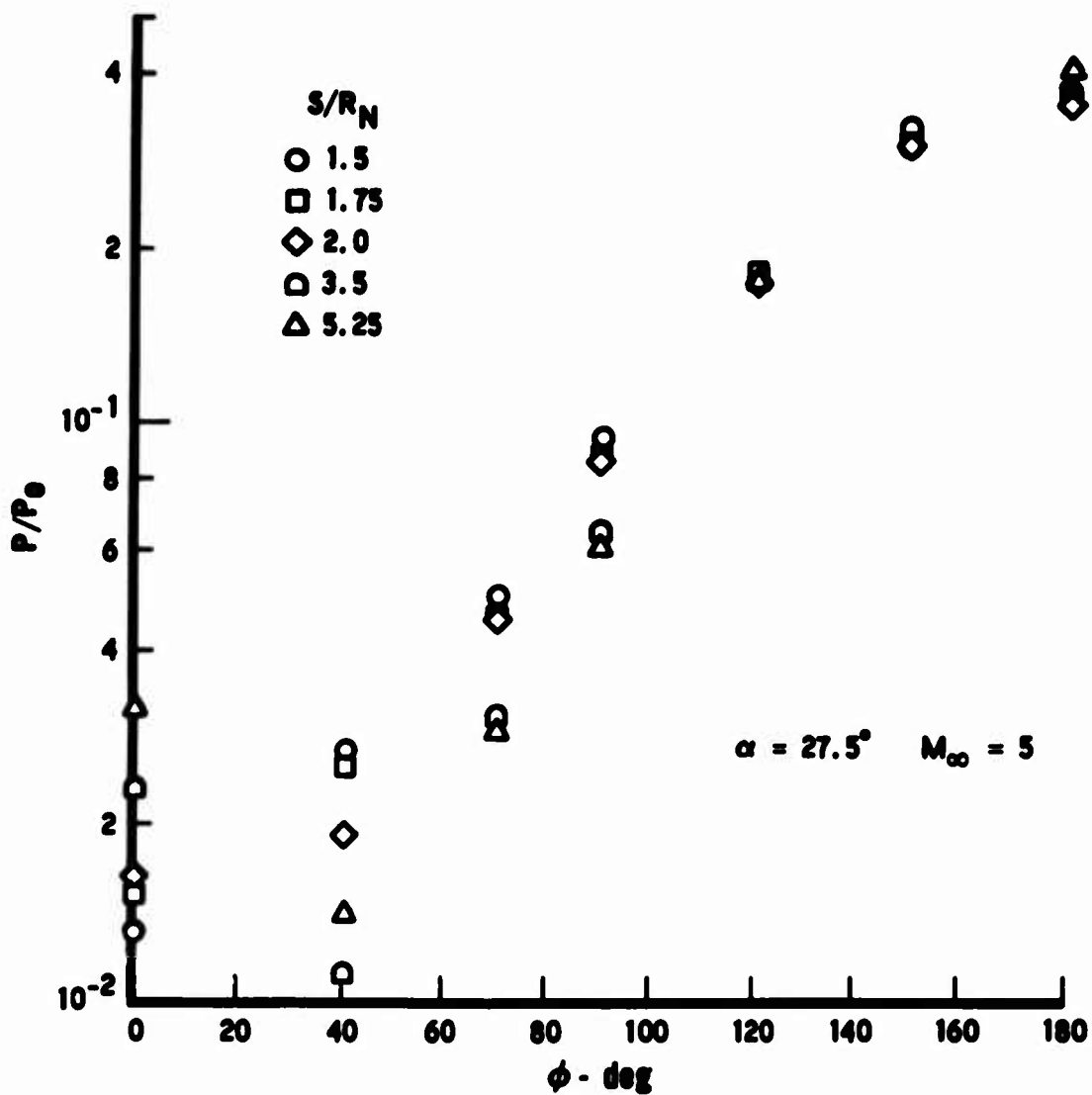


Fig. 11c

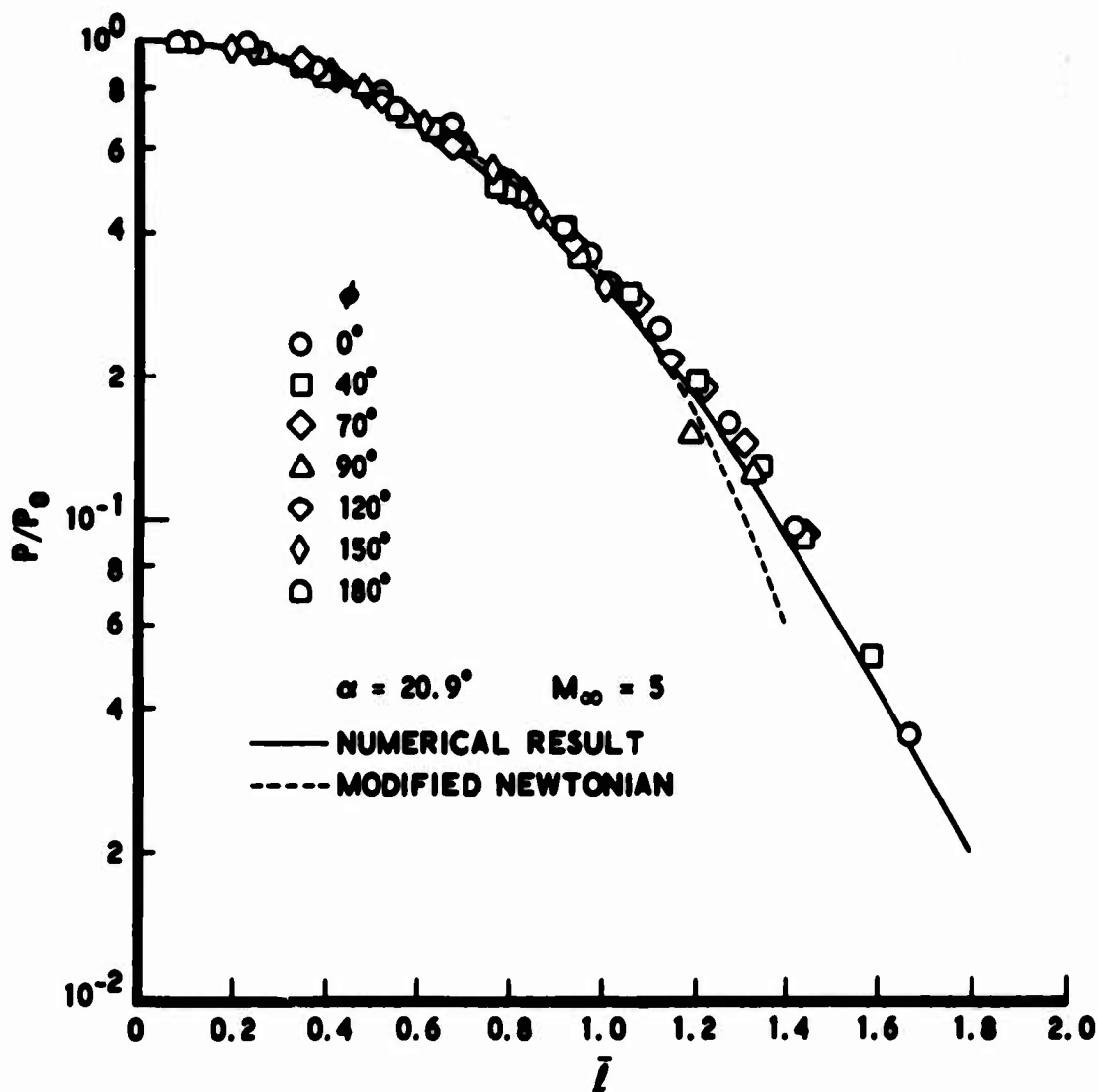


Fig. 12. Pressure Distribution on the Hemispherical Cap

VI. HEAT TRANSFER CORRELATIONS

A convenient and simple correlation of the local nondimensional laminar and turbulent heat transfer rate (q_w/q_{w0}) with the corresponding local surface pressure ratio (p/p_0) for blunt cones at angle of attack was described by the author in Ref. 3. The correlation was demonstrated using two sets of experimental data, one for the laminar and one for the turbulent case. In order to further substantiate some of the conclusions presented therein, the present measurements were analyzed in the same manner.

The laminar correlation presented in Ref. 3 was demonstrated using a set of laminar heat transfer measurements,²⁶ which were obtained over a blunt ($R_N = 0.5$ in.) 25-deg half-angle cone in a $M_\infty = 8$ air flow at freestream Reynolds numbers of 4.0 and $0.89(10)^6$ per foot for an angle-of-attack range of $0 \leq \alpha/\delta_c \leq 2.4$. The turbulent correlation was demonstrated using a set of turbulent measurements¹ obtained over a blunt ($R_N = 2.5$ in.) 9-deg half-angle cone in a $M_\infty = 10.6$ nitrogen flow at a freestream Reynolds number of $12(10)^6$ per foot for an angle-of-attack range of $0 \leq \alpha/\delta_c \leq 2.2$. The resulting correlations for both the laminar and turbulent cases are in terms of sets of power laws (one at each streamwise surface location as measured from the most forward point on the body for a given condition) of the form $\bar{q} = A_g \bar{p}^B$. An individual power law, in a given set, correlates the circumferential laminar or turbulent heat transfer variation at a specific station for a spectrum of angles of attack. For a given flow condition (completely laminar or turbulent), the exponents of the power laws at each station are the same. However, the corresponding exponents for the laminar and turbulent flow cases are different, being 0.74 and 0.96, respectively. The exponents were also shown to be very weak functions of the gas properties γ and ω , where $\mu \propto T^\omega$. Furthermore, it was shown that the coefficient, A_g , could be accurately predicted at each station using the corresponding zero angle-of-attack distribution when it was calculated including the effects of entropy swallowing.

Preceding page blank

Thus, knowing the surface pressure distributions at various angles of attack of interest, together with the zero angle-of-attack heat transfer distribution, the longitudinal and circumferential heat transfer distributions over the entire conical surface at each angle of attack could be generated in a simple fashion. This evaluation would include three-dimensional as well as entropy swallowing effects. The inclusion of these phenomena in any numerical prediction of even a single angle-of-attack heat transfer case is very complicated and costly. Thus, the utility of this type of correlation is immediately obvious and its verification at other conditions is desirable, especially the verification of the apparent independence³ of the power law exponent to variations in Re_∞ , M_∞ , and cone geometry. Since both laminar and turbulent distributions were obtained at the present test conditions, the applicability of both the laminar and turbulent correlations can be determined. Also, since the present test conditions and geometry are different from those corresponding to the initial test results used to establish and demonstrate the correlation, the independence of the exponent, with respect to the aforementioned parameters, can be verified.

A. TURBULENT CASE

The present experimental results were plotted in a manner identical to Ref. 3 to determine if the correlation did indeed apply at the present test conditions. The results are shown in Fig. 13 for the $Re_\infty = 48.5(10)^6$ test condition at stations $S/R_N = 2, 3.5$, and 5.25 . For this particular freestream condition the flow was fully turbulent on the conical surface at each angle of attack. Here it is seen that the present data can also be correlated by a set of power laws, each having the same slope (0.96) determined in Ref. 3. The coefficients, A_g , of each of these curves can

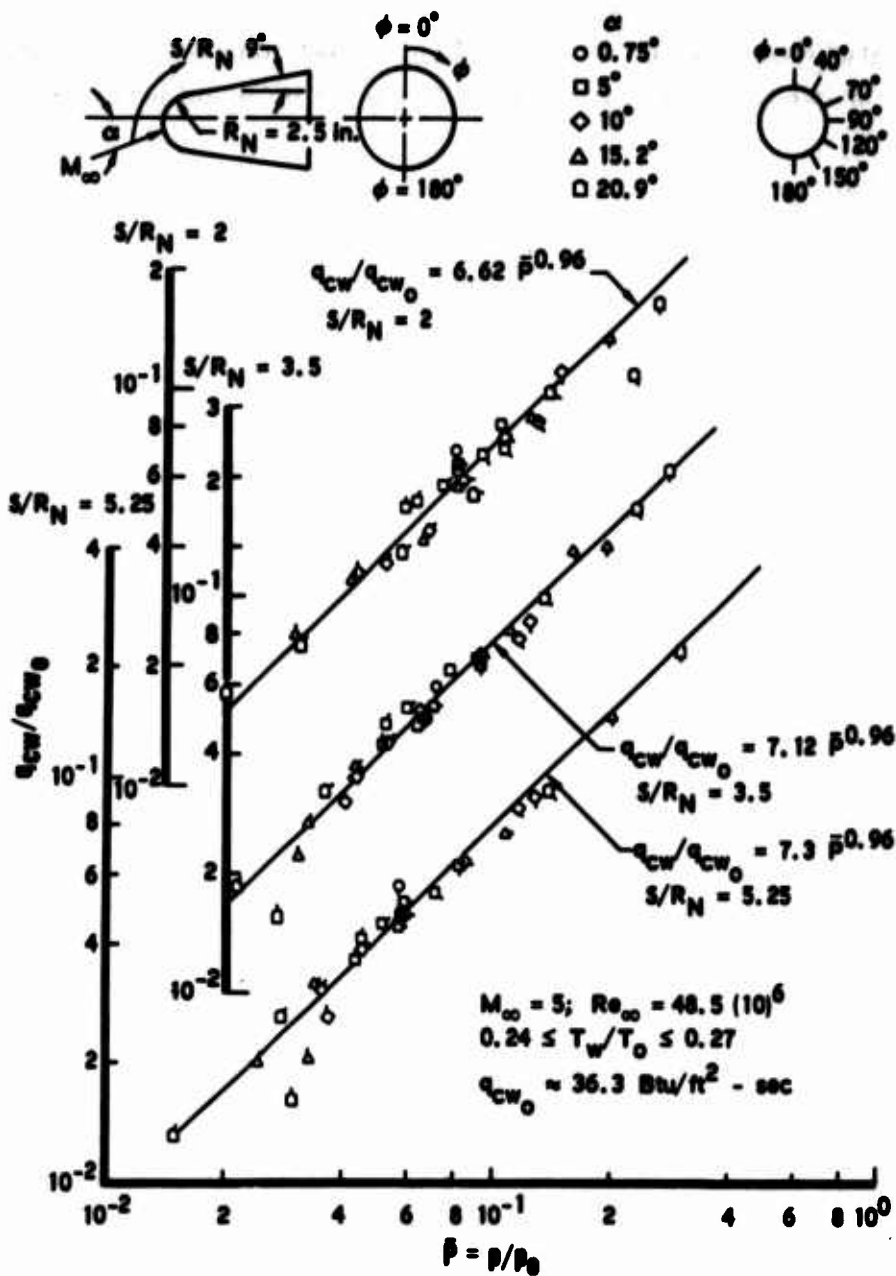


Fig. 13. Correlation of the Turbulent and Heat Transfer Data at Stations $S/R_N = 2, 3.5$, and 5.25

also be predicted by the $\alpha = 0^\circ$ distribution.* Thus, this type of correlation has been shown to be applicable for another set of turbulent heat transfer data.

B. LAMINAR CASE

The laminar data obtained at the $Re_\infty = 4.6(10)^6$ condition are shown at stations $S/R_N = 2, 3.5$, and 5.25 in Figs. 14a-b. The flow is laminar at stations $S/R_N = 2$ and 3.5 for all angles of attack (except for the windward ray at $\alpha = 5^\circ$), and the corresponding data are seen to be correlated by a power law having the same exponent (0.74) determined in Ref. 3. Also, the corresponding power law coefficients, A_s , were found to be predicted fairly accurately by the zero angle-of-attack distribution.† Again, it is pertinent to remember the geometric differences between the two models used in these respective experimental investigations as well as the different freestream conditions and the angle-of-attack range investigated. Thus, the present test results offer further experimental evidence that the exponent is independent of Re_∞ , M_∞ , and the cone geometry.

As the angle of attack was increased, the flow became transitional near the rear of the model, and at station $S/R_N = 5.25$ the flow at some circumferential locations became transitional or fully turbulent. The initial transition occurred on the leeward side for the two higher angle-of-attack tests. Therefore, the corresponding turbulent correlation curve has been included at this station as well as at station $S/R_N = 3.5$. In Fig. 14b, the

* For stations $S/R_N = 3.5$ and 5.25 , the coefficients were determined within 3%, whereas at $S/R_N = 2$, the difference was approximately 12%. The axial distributions indicate that the data at $S/R_N = 2$ are consistently low. This is probably due to the larger conduction error encountered at this station because of its location near a point of discontinuous slope in the heat transfer distribution. Thus, the larger relative disagreement at this station is probably a result of the larger conduction errors present here.

† The coefficients were predicted within 9, 5, and 1.3% at stations $S/R_N = 2, 3.5$, and 5.25 , respectively. The comments made in the previous footnote also apply to this case.

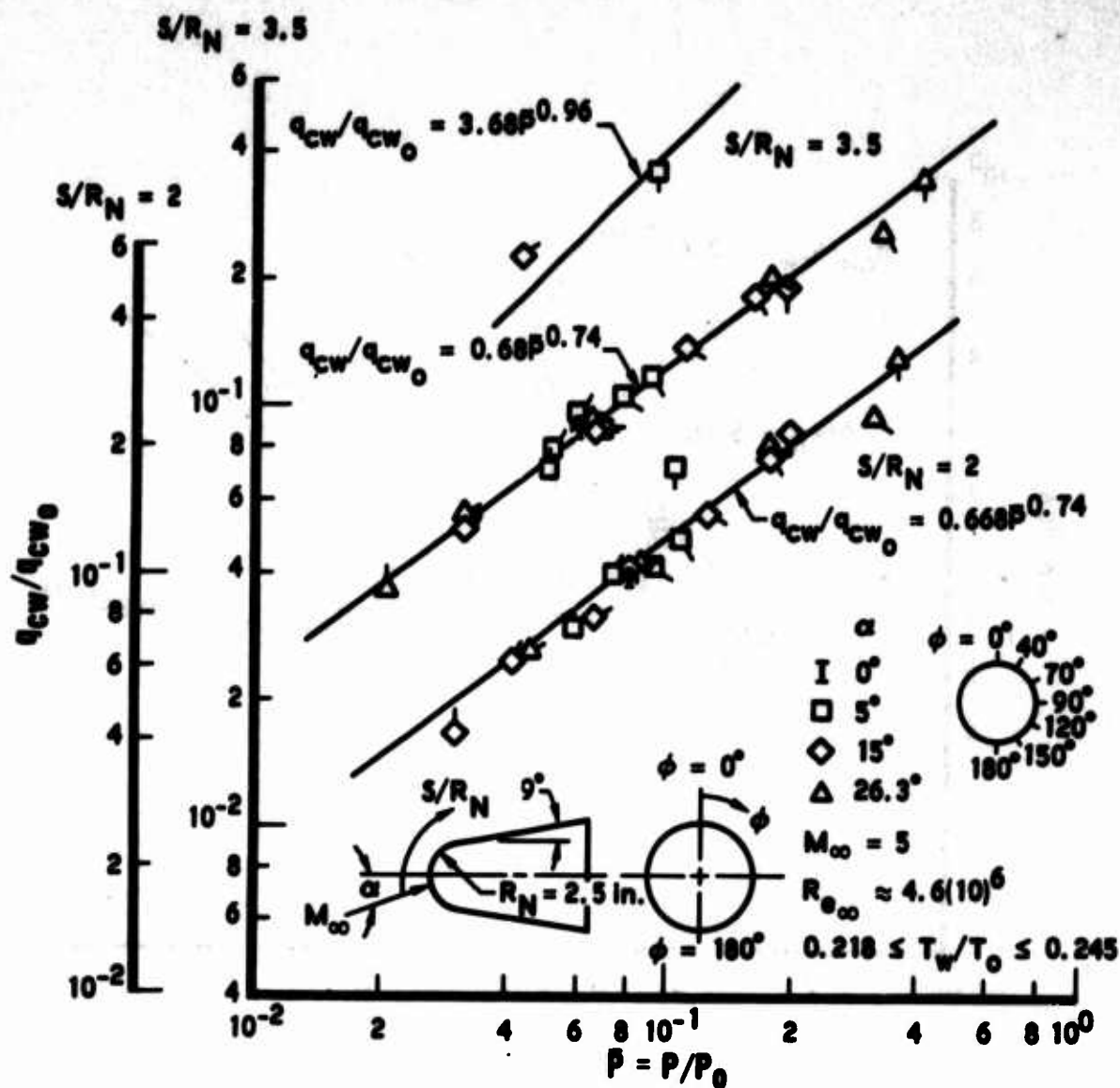


Fig. 14a

Figs. 14. Correlation of the Laminar Heat Transfer Data at Stations $S/R_N = 2, 3.5$, and 5.25

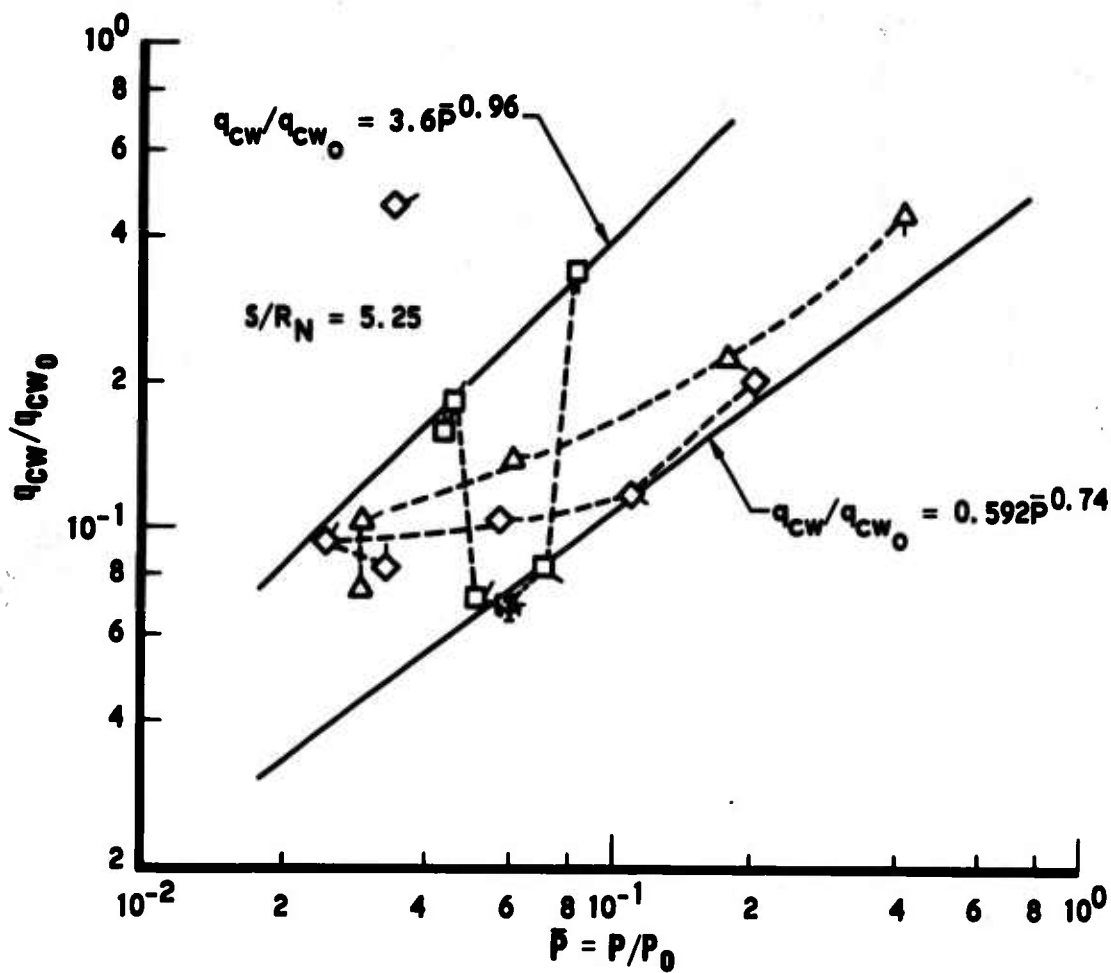


Fig. 14b

circumferential points corresponding to an individual angle of attack have been connected by a dashed line in order to exemplify the circumferential variation of the state of the flow at this station, that is, the variation from the laminar through the transitional to the fully turbulent state. At $\alpha = 15^\circ$, the local state of the flow is seen to progress from the turbulent/transitional condition on the leeward side to the laminar state on the most windward ray. The same type of behavior is apparent for $\alpha = 26.3^\circ$, except that for this case the windward side is in a transitional state. At $\alpha = 5^\circ$, the windward ray is fully turbulent. This behavior may have resulted from a local tripping of the boundary layer by some local disturbance. For the zero angle-of-attack case, the flow was laminar over the entire surface.

It should be noted that the fully turbulent data, as well as the laminar data, are correlated by power laws of the type described in Ref. 3, each having the same exponents as determined in Ref. 3. Thus, the laminar correlation has been verified at this freestream condition, and additional information regarding the turbulent correlation has been obtained as well as an example of the progression from one to the other, via the transitional data.

VII. SUMMARY AND CONCLUSIONS

The results of this investigation can be summarized as follows:

1. Smooth wall turbulent heat transfer measurements at low T_w/T_o ratios were obtained at two freestream conditions [$Re_\infty = 48.5$ and $19(10)^6$] over a range of angles of attack. Natural transition was obtained near the stagnation region at both of these test conditions. Premature transition occurred at the $Re_\infty = 11(10)^6$ test condition. The flow was laminar over the model at the $Re_\infty = 4.6(10)^6$ condition, with transition occurring on the conical surface as the angle of attack was increased.
2. Measurements of the peak turbulent heating were obtained on the hemispherical cap at the $Re_\infty = 48.5(10)^6$ test condition. Detailed measurements of the heat transfer rate were obtained over the entire nosetip at each test condition.
3. Numerical calculations performed using the Vaglio-Laurin turbulent heat transfer relation are in good agreement with the data. Other turbulent heat transfer formulations which were examined did not agree with the data as well as the results obtained using the Vaglio-Laurin relation. Each of these other relations uses reference rather than edge conditions to define the local heat transfer rate. Specifically, the McCuen, et al., and Walker relations substantially overpredict the peak heating for these test conditions and, in general, overpredict the rates on the conical surface as well. The formulation of DeJarnette and Tai yields results for these test conditions which are, in general, a few percent higher than the respective rates calculated using the Vaglio-Laurin relation.
4. Both the turbulent and laminar heat transfer correlations for blunt cones at angle of attack which were previously demonstrated in Ref. 3 were shown to correlate the present data as well. The corresponding power law exponents were found to be the same as those obtained in Ref. 3, providing additional experimental evidence that the exponents are independent of Re_∞ , M_∞ , and the cone geometry. The progression from the laminar to the turbulent correlation curves was demonstrated via the transitional data.
5. Numerical calculations of the surface pressure agree with the measured distributions except in regions where viscous-inviscid interactions become important.

Preceding page blank

APPENDIX A

TEST CONDITIONS AND DATA TABULATIONS

Preceding page blank

Table A-1. Test Conditions - Set 1

Run No.	a	$Re_{\infty}/ft (10)^{-6}$	M_{∞}	P_{∞} (psi)	$\rho_{\infty} \times (10)^{-3}$ (slugs/ft ³)	$T_{O_{\infty}}$ (°R)	$P_{O_{\infty}}$ (psi)	$T_w/T_{O_{\infty}}$	q_{cw0}^* (Btu/ft ² -sec)
29	0.75	47.3	5	2.77	1.75	795.5	1466.1	0.133	36.26
7	5	48.1	5	2.79	1.78	791	1475.2	0.241	36.34
8	10	48.7	5	2.81	1.79	787.9	1484.3	0.260	36.31
9	15.2	49.4	5	2.78	1.80	776.1	1470.6	0.271	35.48
10	20.9	48.6	5	2.78	1.79	785.3	1472.8	0.265	35.96

* Calculated using the Fay and Riddell relation (Ref. 13).

Table A-2. Heat Transfer Data - Set 1

S/R_N	ϕ (deg)	q_{cw} (Btu/ft ² -sec)				
		Run No.				
		29	7	8	9	10
0.0	0		37.120	55.860		98.740
0.15	0	35.300	47.601	79.469	93.696	97.600
	90	35.300	37.790	70.000	85.000	97.600
	180	35.300	34.800	40.000	69.501	92.844
0.30	0		70.200	87.300	89.154	98.200
	40		75.960	87.385	87.562	90.000
	70		61.500	79.700	82.361	91.425
	90					
	120		37.757	47.800	64.003	80.816
	150		33.560	31.930		73.600
	180		32.760	31.800	35.433	69.450
0.45	0	76.600	86.099	93.855	91.073	89.828
	90	78.600	79.700	91.700	89.054	96.917
	180	85.400	67.500	49.235	30.500	32.200
0.60	0	92.957	89.674	88.861	83.520	80.100
	40		95.610	95.200	84.410	87.401
	70		89.842	91.759	87.211	92.622
	90		86.338	93.200	88.921	91.600
	120		83.807	90.900	84.524	88.184
	150		84.330	86.924		
	180	86.531	84.300	82.700	64.343	41.469
0.75	0		77.851	76.400	65.052	58.000
	90	75.100	78.050	84.500	77.225	77.616
	180	74.700	79.000	82.700	71.934	66.170
0.90	0	71.600	65.300	62.400	49.699	41.678
	40		67.600	61.600		45.000
	70	68.700	71.150	72.000	65.600	63.000
	90	68.300	70.900	72.800	68.981	68.894
	120		75.262			71.600
	150		79.982	84.286	84.945	82.304
	180	68.300	75.600	82.600	77.859	76.474

Table A-2. Heat Transfer Data - Set 1 (Continued)

S/R _N	φ (deg)	q _{cw} (Btu/ft ² -sec)				
		Run No.				
		29	7	8	9	10
1.05	0	55.600	51.547	44.400	35.589	27.600
	40		51.200	44.800		30.580
	70		54.300	51.700	47.325	43.773
	90	56.300	56.900	58.600	54.541	52.979
	120		58.500	62.800	66.850	67.100
	150		56.700	65.000		59.000
	180		62.000	70.600	71.600	75.400
1.30	0	42.100	36.464	27.200	21.717	17.255
	40		33.600	28.160		
	70		34.300	32.400	30.100	26.819
	90	41.700	38.700	45.100	38.500	38.465
	120		42.580	49.300	50.137	57.170
	150		44.100	53.000		
	180	40.500	45.600	54.200	59.514	64.824
1.50	0	24.050	18.542	13.070	8.740	6.730
	40		18.800	14.980	12.341	8.883
	70		22.100	19.700	16.197	14.425
	90	26.000	24.700	24.000	23.132	21.809
	120		27.550	28.100	32.851	35.411
	150		28.900	38.000		49.700
	180	25.950	29.400	35.700	41.450	52.900
2.00	0		18.030	12.245	8.297	6.022
	40			12.700		
	70		20.650	15.732	14.635	13.273
	90					
	120		24.640	27.500	30.427	34.947
	150		26.300	30.350		43.400
	180	25.500	29.933	38.800	46.020	57.739
3.50	0	18.130	15.397	11.042	7.872	5.540
	40		17.264	13.001	9.350	6.376
	70		19.230	15.750	13.275	11.380
	90		19.600	18.800	17.600	17.209
	120		24.003	26.500	29.500	35.792
	150		25.300	28.300	40.201	52.332
	180	21.650	25.180	32.300	40.700	54.400

Table A-2. Heat Transfer Data - Set 1 (Concluded)

S/R_N	ϕ (deg)	q_{cw} (Btu/ft ² -sec)				
		Run No.				
		29	7	8	9	10
5.25	0	17.300	13.300	9.158	6.990	5.789
	40		14.770	10.472	6.695	3.834
	70		16.230	13.900	11.070	9.070
	90		18.430	17.170	16.524	16.021
	120		20.050	24.000	27.250	35.200
	150		21.710	31.580	35.200	
	180	20.087	22.900	34.000	42.900	57.500

Table A-3. Test Conditions — Set 2

Run No.	a	$Re_{\infty}/ft (10)^{-6}$	M_{∞}	P_{∞} (psi)	$\rho_{\infty} \times (10)^{+4}$ (slugs/ft ³)	$T_{O_{\infty}}$ (°R)	$P_{O_{\infty}}$ (psi)	$T_w/T_{O_{\infty}}$	q_{cw}^* (Btu/ft ² -sec)
20	0	18.3	5	1.07	6.79	797.1	568.4	0.232	22.93
19	5	19.3	5	1.09	7.08	778.7	579.1	0.229	22.3
21	10	18.3	5	1.07	6.81	784.4	555.1	0.242	22.06
12	15	19.5	5	1.09	7.11	773.9	577.9	0.208	22.18
22	20.25	19.3	5	1.08	7.05	773.9	572.9	0.256	22.07
23	27.5	18.8	5	1.10	6.95	794.5	580	0.283	22.91

* Calculated using the Fay and Riddell relation (Ref. 13).

Table A-4. Heat Transfer Data - Set 2

S/R _N	φ (deg)	q _{cw} (Btu/ft ² -sec)					
		Run No.					
		20	19	21	12	22	23
0.0	0	20.7	21.400	19.080	33.370	22.000	34.200
0.15	0	22.779	20.460	18.665	43.727	26.700	38.200
	90	23.516	21.306	19.360	38.900	18.450	26.700
	180	23.483	22.333	18.800	34.100	19.032	20.147
0.30	0	19.542	18.014	16.451	43.226	36.092	39.400
	40		16.960	16.200	37.500	31.600	22.197
	70	18.831	18.410	15.918	39.832	19.031	19.911
	90						
	120	18.350	18.630	16.218	28.000	15.923	16.520
	150		17.420	16.190	21.610	16.030	16.450
	180	19.628	19.755	17.185	20.200	17.353	17.300
0.45	0	21.484	25.097	27.428	43.270	43.646	37.600
	90	19.793	20.000	18.211	42.807	27.577	29.400
	180	19.459	17.721	15.300	20.200	19.160	17.830
0.60	0	35.964	41.367	39.042	39.280	33.564	30.900
	40	37.500	48.200	43.890	41.764	47.345	40.230
	70	34.700	42.400	36.738	44.126	43.621	47.000
	90	39.116	39.300	29.900	43.328	42.811	43.800
	120	33.900	25.943	19.167	40.134	19.506	16.260
	150						
	180	26.400	18.936	15.300	26.500	17.282	18.194
0.75	0	41.400	37.300	33.700	31.200	25.700	20.221
	90	41.608	42.600	39.300	37.642	36.500	33.500
	180	41.700	25.500	14.700	33.500	15.286	15.877
0.90	0	39.800	29.900	25.800	23.857	18.972	13.970
	40		30.350	26.650	25.010	20.000	16.040
	70	41.964	33.700	32.159	32.000	27.908	24.047
	90	41.200	31.114	38.365	34.000	30.940	35.013
	120						
	150		34.900	37.750	36.500	25.390	16.100
	180	34.600	38.866	26.711	41.163	16.819	15.404

Table A-4. Heat Transfer Data - Set 2 (Continued)

S/R _N	φ (deg)	q _{cw} (Btu/ft ² -sec)					
		Run No.					
		20	19	21	12	22	23
1.05	0	31.600	23.240	19.900	16.800	13.943	9.340
	40		22.600	20.326	18.400	14.830	11.330
	70	31.698	25.042		24.400	21.000	18.297
	90		26.378	30.500	28.200	25.218	25.300
	120		27.700	30.912	30.800	30.053	40.345
	150			31.300	31.000	31.000	21.300
	180	31.700	34.700	33.733	36.500	32.000	13.959
1.30	0	18.447	17.202	11.900	11.046	8.341	5.810
	40	18.900	17.490	14.096	11.315	9.845	7.560
	70	21.447	18.365	14.579	15.790	14.500	12.056
	90	18.515	20.860	18.900	19.700	18.360	18.837
	120	19.029	21.713	23.100	24.600	26.490	27.560
	150	19.280	23.850	23.800	25.600	35.300	26.500
	180	20.576	23.800	28.212	28.700	37.476	19.000
1.50	0	12.060	9.355	6.730	5.028	2.920	0.069
	40	12.500	9.850	8.230	5.658	4.607	2.990
	70	11.680	10.438	9.190	8.335	7.588	6.224
	90	12.470	12.265	11.800	11.551	11.736	10.743
	120	12.264	13.068	14.561	15.198	19.300	19.573
	150						28.000
	180	11.442	15.493	18.350	24.000	28.907	37.800
2.00	0	11.908	8.863	6.430	4.343	3.370	1.634
	40		9.430	7.705	13.000	9.280	7.080
	70	11.159	9.224	6.852	7.494	6.010	4.476
	90						
	120	11.298	12.300	13.819	15.402	16.598	19.644
	150		11.500	14.300	15.970	19.950	25.000
	180	11.950	15.321	18.515	22.825	27.559	36.812
3.50	0	9.954	7.080	5.880	3.680	3.139	2.250
	40	10.300	8.090	6.340	4.760	3.283	1.731
	70	10.900	9.648	6.293	6.760	4.711	3.980
	90	9.650	9.118	7.610	8.731	7.762	7.310
	120	10.000	11.475	12.209	14.620	16.915	19.072
	150	9.561	12.304	14.479	19.556	23.120	29.877
	180	9.550	12.151	14.561	22.400	24.162	31.790

Table A-4. Heat Transfer Data - Set 2 (Concluded)

S/R _N	φ (deg)	q _{cw} (Btu/ft ² -sec)					
		Run No.					
		20	19	21	12	22	23
5.25	0	8.270	6.079	4.030	3.890	2.836	3.168
	40	8.760	6.690	4.361	5.230	2.020	0.715
	70	8.807	7.434	6.086	7.180	4.144	3.490
	90	8.300	8.332	7.330	7.717	7.541	7.259
	120	8.760	10.284	10.208	12.676	15.652	20.195
	150	8.704	11.817	14.566	21.550	25.490	33.486
	180	7.967	11.340	14.700	23.820	33.300	41.100

Table A-5. Test Conditions — Set 3

Run No.	α	$Re_{\infty}/ft (10)^{-6}$	M_{∞}	P_{∞} (psi)	$\rho_{\infty} \times (10)^{+4}$ (slugs/ft ³)	$T_{O_{\infty}}$ (°R)	$P_{O_{\infty}}$ (psi)	$T_w/T_{O_{\infty}}$	q_{cw}^* (Btu/ft ² -sec)
13	0	11	5	0.64	4.06	789.2	336.6	0.19	17.34
16	5	11.6	5	0.64	4.21	764.7	338.4	0.232	16.74
17	10	11	5	0.64	4.05	792.7	377.5	0.224	17.44
14	15	10.8	5	0.64	4.03	800.2	338.4	0.20	17.61
18	20.25	10.8	5	0.64	4.03	799.3	338.4	0.266	17.61
15	26.5	10.7	5	0.65	4.01	812.4	342	0.258	18.08

* Calculated using the Fay and Riddell relation (Ref. 13).

Table A-6. Heat Transfer Data - Set 3

S/R _N	φ (deg)	q _{cw} (Btu/ft ² - sec)					
		Run No.					
		13	16	17	14	18	15
0.0	0	17.520	16.520	16.730	18.960	20.550	27.850
0.15	0	17.900	16.484	16.859	21.521	30.950	34.809
	90	17.593	16.026	15.380	17.667	21.415	31.100
	180	17.224	16.500	15.780	15.900	17.440	29.800
0.30	0	15.351	15.652	17.704	26.357	29.600	30.100
	40	14.054	14.700	15.740	24.300	21.842	22.878
	70	15.797	14.802	16.200	20.250	25.900	30.762
	90						
	120	14.317	13.680	14.116	14.624	15.709	24.061
	150		13.740	13.990	14.150	13.620	19.420
	180	15.918	15.350	14.750	14.568	13.900	18.272
0.45	0	22.076	28.100	29.337	28.759	28.400	26.100
	90		21.050	19.888	25.032	27.100	32.300
	180	20.850	14.823	14.750	14.681	14.200	15.245
0.60	0	27.400	27.200	26.189	26.776	24.202	19.500
	40	29.600	29.600	30.500	30.900	28.000	25.700
	70	27.209	26.438	26.994	28.208	27.514	28.339
	90	26.650	27.100	25.837	27.955	28.800	28.962
	120	26.780	26.800	24.800	26.184	24.819	28.877
	150						
	180	28.244	25.200	15.630	15.000	13.950	14.331
0.75	0	25.200	24.100	21.317	21.733	16.900	13.410
	90	25.574	24.700	24.594	25.395	24.250	23.900
	180	25.000	24.500	21.906	19.709	13.520	12.690
0.90	0	23.382	20.100	17.830	16.550	12.280	9.606
	40	22.800	19.640	18.530	18.280	14.220	12.500
	70	23.728	21.400	21.600	21.394	10.510	18.384
	90	23.592	21.738	22.374	23.056	21.600	21.027
	120						
	150	25.388	24.400	23.820	23.800	22.250	21.923
	180	24.200	24.400	23.652	27.569	21.300	18.606

Table A-6. Heat Transfer Data - Set 3 (Continued)

S/R _N	φ (deg)	q _{cw} (Btu/ft ² -sec)					
		Run No.					
		13	16	17	14	18	15
1.05	0	18.440	15.540	12.564	11.300	7.421	6.349
	40		15.260	15.400	12.430	10.000	7.800
	70	18.610	16.330	16.721	15.825	14.180	12.416
	90	18.803	19.500	18.276	19.350	17.470	16.839
	120	18.829	19.000	19.538	20.865	20.400	20.972
	150			19.700	20.600	19.320	21.100
	180	18.800	19.600	20.645	22.410	24.300	22.850
1.30	0	13.879	10.353	8.900	7.396	4.684	3.956
	40	12.350	10.520	9.426	8.000	6.210	4.430
	70	12.680	11.550	11.165	10.289	7.430	8.000
	90	14.105	12.640	13.180	13.284	13.050	11.067
	120	14.268	13.400	14.800	16.804	16.150	11.957
	150		13.420	17.300	18.130	17.280	20.000
	180	14.437	15.800	17.560	18.611	20.000	21.459
1.50	0	7.920	6.050	4.330	2.585		0.931
	40	7.930	6.219	4.810	4.376	2.400	1.385
	70	7.833	7.040	6.200	6.041	4.540	3.776
	90	7.970	7.400	8.179	7.850	6.930	6.665
	120	7.950	8.290	10.272	11.440	12.900	13.800
	150				12.000		17.750
	180	7.888	9.820	12.224	15.300	16.200	21.053
2.00	0	7.550	5.500	4.240	2.884	2.003	0.236
	40	8.479	6.394	6.470	7.684	8.116	8.717
	70	7.310	6.110	5.920	5.297	4.270	3.886
	90						
	120	7.771	7.850	9.233	10.698	11.800	12.428
	150		8.000	9.200	12.000	13.250	16.130
	180	8.356	9.652	12.846	15.800	17.130	21.055
3.50	0	6.463	4.619	3.700	2.948	1.760	1.200
	40	7.083	4.927	4.180	3.440	1.897	1.186
	70	6.560	5.998	5.430	4.800	3.758	2.920
	90	6.114	5.900	5.994	6.109	5.600	5.197
	120	6.327	6.925	8.485	9.600	10.817	12.304
	150	6.110		9.945	12.400	15.300	19.409
	180	6.350	7.570	10.149	13.250	16.900	21.031

Table A-6. Heat Transfer Data - Set 3 (Concluded)

S/R _N	φ (deg)	q _{cw} (Btu/ft ² -sec)					
		Run No.					
		13	16	17	14	18	15
5.25	0	5.501	3.785	3.160	2.610	1.818	2.030
	40	5.640	3.842	3.557	2.608	1.616	0.270
	70	5.640	4.570	4.247	3.397	2.621	2.037
	90	5.476	5.044	5.407	5.600	5.040	5.347
	120	5.776	6.279	8.030	8.814	9.931	12.045
	150	5.710	7.169	10.512	13.441	17.729	22.010
	180	5.369	6.954	10.841	14.539	18.600	23.100

Table A-7. Test Conditions - Set 4

Run No.	α	$Re_{\infty}/ft (10)^{-6}$	M_{∞}	P_{∞} (psi)	$\rho_{\infty} \times (10)^{+4}$ (slugs/ft ³)	$T_{o\infty}$ ($^{\circ}R$)	$P_{o\infty}$ (psi)	$T_w/T_{o\infty}$ (nominal)	q_{cw}^* $q_{o\infty}$ (Btu/ft ² -sec)
24	0	4.53	5	0.28	1.71	816.5	146.5	0.218	11.93
25	5	4.56	5	0.28	1.71	813.6	146.6	0.235	11.88
26	15	4.72	5	0.28	1.76	804.4	148.8	0.235	11.75
27	26.3	4.74	5	0.28	1.77	808.3	150.6	0.245	11.8

* Calculated using the Fay and Riddell relation (Ref. 13).

Table A-8. Heat Transfer Data - Set 4

S/R _N	φ (deg)	q _{cw} (Btu/ft ² - sec)			
		Run No.			
		24	25	26	27
0.0	0	10.862	11.262	10.696	9.720
0.15	0	11.000	10.485	9.310	8.994
	90	11.325	10.600	9.560	8.912
	180	10.899	10.870	10.128	9.716
0.30	0		8.300	8.080	6.460
	40		7.650	8.290	5.815
	70	9.400	9.356	8.327	7.710
	120	9.400	9.110	9.260	8.200
	150		9.190	8.908	
	180	9.810	9.640	9.872	9.194
0.45	0	9.420	8.210	7.160	5.683
	90		8.932	7.910	7.323
	180	8.820	9.232	9.484	
0.60	0	8.000	7.320	5.550	4.240
	40	8.000	7.530	5.670	5.250
	70	7.923	7.916	6.860	5.978
	120	8.080	7.890	8.222	7.650
	180	8.000	8.160	8.942	9.901
0.75	0	6.685	5.871	4.390	3.480
	90	6.732	6.360	5.661	5.340
	180	6.472	6.555	7.840	8.567
0.90	0	5.620	4.821	3.617	2.450
	40		4.810	3.938	3.000
	70	5.630	4.670	4.242	4.040
	90	5.559	4.819	4.830	4.650
	120			6.600	
	150		5.750	2.845	7.880
	180	5.490	5.570	7.260	8.259

Table A-8. Heat Transfer Data - Set 4 (Continued)

S/R _N	φ (deg)	q _{cw} (Btu/ft ² - sec)			
		Run No.			
		24	25	26	27
1.05	0	4.380	3.500	2.415	1.616
	40		3.590		2.025
	70	4.081	3.660	3.237	2.420
	90	4.320	3.900	4.240	
	120	4.367	4.026	4.727	5.005
	150		4.410		
	180	4.320	4.539	5.650	6.950
1.30	0	3.030	2.457	1.810	1.010
	40	2.790	2.360		
	70	2.735	2.424	2.436	1.602
	90	2.798	2.680	2.740	2.585
	120	2.779	3.010	3.782	4.170
	150			4.035	4.811
	180	3.100	3.221	4.698	5.575
1.50	0		1.055	0.604	0.940
	40	1.520	1.260	0.763	
	70	1.493	1.342	1.013	0.709
	90	1.419	1.420	1.382	1.372
	120	1.539	1.628	2.010	2.580
	150		1.707		
	180	1.470	1.930	2.871	4.215
2.00	0	1.180	0.854	0.402	0.197
	40		2.640	2.335	2.060
	70		1.162	0.885	0.760
	90				
	120	1.175	1.220	1.612	2.380
	150		1.425	2.215	2.840
	180	1.182	2.030	2.652	3.960
3.50	0	1.018	0.837		0.404
	40	1.018	0.925	0.587	0.301
	70	1.085	1.140	2.780	0.622
	90	1.058	1.010	1.005	1.090
	120	1.085	1.260	1.610	2.385
	150	1.018	1.350	2.130	2.780
	180	1.029	4.270	2.217	3.956

Table A-8. Heat Transfer Data - Set 4 (Concluded)

S/R_N	ϕ (deg)	q_{cw} (Btu/ft ² - sec)			
		Run No.			
		24	25	26	27
5.25	0	0.817	1.990	1.150	1.210
	40		2.290	1.280	
	70	0.792	0.854	5.640	1.332
	90	0.817	0.814	1.205	1.610
	120	0.775	0.975	1.410	2.590
	150	0.784	4.280	2.010	4.680
	180	0.817	4.070	2.366	4.850

Table A-9. Pressure Data

S/R _N	ϕ (deg)	P/P ₀					
		α (deg)					
		0	5	10	15.4	20.9	27.5
0.0	0	0.963	0.944	0.955	0.919	0.872	0.784
0.15	0	0.992	0.950	0.899	0.835	0.771	0.672
	90	0.997	0.986	0.937	0.903	0.852	0.784
	180	0.983	0.997	1.007	1.008	0.989	0.899
0.30	0	0.929	0.861	0.686	0.743	0.665	0.531
	40	0.915	0.870	0.787	0.724	0.652	0.563
	70	0.896	0.862	0.834	0.789	0.731	0.664
	90	0.919	0.907	0.871	0.829	0.784	0.749
	120	0.907	0.923	0.921	0.928	0.903	0.851
	150	0.938	0.971	0.977	0.969	0.966	0.958
	180	0.925	0.974	0.992	0.985	0.983	0.994
0.45	0	0.792	0.711	0.602	0.548	0.475	0.384
	40	0.780	0.713	0.648	0.568	0.497	0.440
	70	0.770	0.726	0.698	0.655	0.609	0.522
	90	0.807	0.799	0.751	0.721	0.679	0.647
	120	0.797	0.824	0.835	0.837	0.834	0.816
	150	0.804	0.862	0.898	0.928	0.950	0.984
	180	0.804	0.874	0.907	0.948	0.978	1.006
0.60	0	0.679	0.595	0.500	0.435	0.358	0.273
	40	0.656	0.623	0.538	0.475	0.406	0.321
	70	0.676	0.640	0.598	0.560	0.504	0.430
	90	0.683	0.674	0.645	0.634	0.598	0.545
	120	0.685	0.721	0.724	0.751	0.756	0.760
	150	0.690	0.759	0.783	0.852	0.879	0.937
	180	0.685	0.767	0.826	0.895	0.944	1.000

Table A-9. Pressure Data (Continued)

S/R_N	ϕ (deg)	P/P_0					
		α (deg)					
		0	5	10	15.4	20.9	27.5
0.75	0	0.545	0.460	0.375	0.313	0.250	0.183
	40	0.544	0.473	0.399	0.349	0.295	0.226
	70	0.545	0.509	0.461	0.412	0.374	0.336
	90	0.547	0.539	0.517	0.510	0.483	0.434
	120	0.576	0.615	0.618	0.635	0.644	0.676
	150	0.542	0.613	0.675	0.729	0.781	0.861
	180	0.536	0.620	0.701	0.782	0.851	0.949
0.90	0	0.398	0.326	0.253	0.208	0.159	0.109
	40	0.400	0.341	0.152	0.236	0.195	0.145
	70	0.405	0.376	0.337	0.316	0.285	0.243
	90						
	120	0.404	0.443	0.449	0.503	0.522	0.541
	150	0.408	0.474	0.546	0.611	0.668	0.742
	180	0.407	0.487	0.569	0.650	0.733	0.834
1.05	0	0.279	0.219	0.169	0.130	0.096	0.064
	40	0.281	0.233	0.193	0.158	0.127	0.096
	70	0.279	0.256	0.235	0.210	0.190	0.166
	90						
	120	0.282	0.323	0.342	0.387	0.411	0.431
	150	0.288	0.346	0.399	0.475	0.540	0.615
	180	0.293	0.359	0.437	0.527	0.606	0.712

Table A-9. Pressure Data (Continued)

S/R_N	ϕ (deg)	P/P_0					
		α (deg)					
		0	5	10	15.4	20.9	27.5
1.15	0						
	40	0.216	0.175	0.142	0.114	0.091	0.068
	70	0.211	0.190	0.172	0.157	0.143	0.123
	90	0.163	0.133	0.232	0.153	0.150	0.150
	120	0.213	0.240	0.265	0.295	0.317	0.344
	150	0.215	0.261	0.310	0.375	0.438	0.518
	180	0.218	0.277	0.334	0.416	0.492	0.619
1.30	0	0.129	0.096	0.072	0.051	0.035	0.021
	40	0.131	0.103	0.084	0.064	0.051	0.036
	70	0.135	0.121	0.110	0.100	0.093	0.081
	90	0.129	0.129	0.128	0.125	0.124	0.122
	120	0.129	0.148	0.170	0.194	0.216	0.243
	150	0.129	0.169	0.203	0.259	0.308	0.382
	180	0.142	0.187	0.229	0.289	0.356	0.480
1.50	0	0.085	0.060	0.044	0.029	0.019	0.013
	40	0.086	0.067	0.053	0.041	0.031	0.027
	70	0.084	0.075	0.069	0.059	0.058	0.050
	90	0.088	0.087	0.088	0.086	0.088	0.095
	120	0.084	0.098	0.117	0.135	0.155	0.178
	150	0.084	0.113	0.146	0.184	0.231	0.300
	180	0.081	0.117	0.158	0.205	0.262	0.381

Table A-9. Pressure Data (Continued)

S/R_N	ϕ (deg)	P/P_0					
		α (deg)					
		0	5	10	15.4	20.9	27.5
1.75	0	0.082	0.059	0.034	0.030	0.021	0.015
	40	0.084	0.066	0.053	0.041	0.031	0.025
	70	0.085	0.075	0.069	0.065	0.058	0.046
	90	0.084	0.082	0.085	0.085	0.090	0.087
	120	0.082	0.086	0.114	0.131	0.151	0.181
	150	0.087	0.117	0.142	0.185	0.232	0.307
	180	0.085	0.119	0.150	0.208	0.267	0.369
2.00	0	0.081	0.058	0.043	0.029	0.021	0.016
	40	0.079	0.062	0.051	0.040	0.029	0.019
	70	0.081	0.073	0.067	0.067	0.055	0.045
	90	0.080	0.080	0.083	0.081	0.088	0.086
	120	0.081	0.094	0.109	0.127	0.148	0.175
	150	0.084	0.111	0.135	0.179	0.225	0.307
	180	0.080	0.106	0.149	0.198	0.260	0.356
3.50	0	0.067	0.051	0.040	0.032	0.029	0.023
	40	0.068	0.052	0.043	0.031	0.020	0.011
	70	0.069	0.059	0.053	0.042	0.035	0.031
	90	0.067	0.070	0.065	0.066	0.063	0.065
	120	0.066	0.077	0.092	0.110	0.135	0.174
	150	0.071	0.091	0.118	0.159	0.225	0.322
	180	0.059	0.093	0.128	0.188	0.274	0.404

Table A-9. Pressure Data (Concluded)

S/R_N	ϕ (deg)	P/P_0					
		α (deg)					
		0	5	10	15.4	20.9	27.5
5.25	0	0.058	0.043	0.037	0.032	0.030	0.032
	40	0.056	0.045	0.035	0.024	0.013	0.014
	70	0.059	0.051	0.045	0.034	0.028	0.029
	90	0.059	0.059	0.059	0.057	0.057	0.061
	120	0.062	0.071	0.085	0.108	0.138	0.176
	150			0.117			
	180	0.057	0.083	0.123	0.201	0.296	0.411

APPENDIX B

DATA REDUCTION TECHNIQUE

The thin-skinned calorimeter technique/concept was used to reduce the transient temperature response of each thermocouple to a corresponding local heat transfer rate. In this technique, each element of the thin-wall model is assumed to act as a calorimeter and all heat transfer rates other than the boundary layer surface heat transfer (q_w) are neglected. Therefore, the heat balance for a specific calorimeter element can be written in the form

$$q_w = \rho_m C_{p_m} \delta \frac{\partial T}{\partial t} \quad (B-1)$$

where δ is implicitly considered to be thin enough so that the specific element can be assumed to be at a uniform temperature instantaneously.

Defining the heat transfer coefficient, h , as

$$h = \frac{q_w}{T_r - T_w} \quad (B-2)$$

this balance becomes

$$h = \frac{\rho_m C_{p_m} \delta}{T_r - T_w} \frac{\partial T}{\partial t} \quad (B-3)$$

Various methods are available for transforming the aforementioned transient temperature data, which were recorded at finite time intervals during the specific tests, to a form that can be used in Eq. (B-3) to obtain

the local heat transfer coefficient. The accuracy of fitting a polynomial to the transient temperature data and then differentiating to obtain $\partial T/\partial t$ was investigated in Ref. 8. There it was compared to a different technique developed in Ref. 7, termed the "stepwise integration" technique, and found to yield less accurate results. Thus, the "stepwise integration" technique was used to reduce the present data. The technique is briefly described in the following section together with the possible sources of error encountered in transforming the thermocouple response to a local heat transfer coefficient using the techniques described herein.

Since ρ and $\delta(x)$ are known, if C_{pm} is represented by a linear function $A + BT$ over the temperature range defined by a small time interval Δt , Eq. (B-3) can be integrated to yield

$$h = \frac{\rho_m \delta C_{pm}}{\Delta t} \left\{ (A + BT_r) \ln \left[\frac{T_r - T_1}{T_r - T_2} \right] - B(T_1 - T_2) \right\} \quad (B-4)$$

if, in addition, h is assumed to be constant over the same small time interval. Under these assumptions, the resulting value of h is taken to be representative of the heat transfer coefficient at the mean of the specific interval, Δt .

Thus, knowing the C_{pm} variation, model material, and the transient backface temperature response as measured by the individual thermocouples, the local heat transfer coefficient can be obtained by using Eq. (B-4). However, the subsequent evaluation of the heat transfer coefficient in the aforementioned manner is subject to error⁸ arising from

- (a) evaluation of the physical properties of the material [ρ_m and $C_{pm}(T)$]
- (b) variation of the wall thickness at each station, $\delta(x)$
- (c) radiation effects
- (d) neglect of surface curvature
- (e) nonuniform precooling

- (f) nonuniform heating of the model when it passes through the tunnel shear layer as it is being injected into test section
- (g) thermocouple losses
- (h) impressed conduction in the normal, longitudinal, and circumferential directions
- (i) assumptions inherent in the stepwise integration data reduction technique.

Each source of error was examined, and its impact on the resulting reduced heat transfer data is discussed below. Here the general results reported in Ref. 8 were used to evaluate the order of the aforementioned errors.

(a) Physical Properties

The material density is known, $\rho_m = 490.75 \text{ lb/ft}^3$. The variation of C_{p_m} with temperature was obtained from measurements made on the same type of material used to fabricate the present model and are considered to be the best available data. These data are discussed in Ref. 10.

(b) Wall Thickness

The wall thickness, δ , was measured at each thermocouple location and used in the determination of the local heat transfer coefficient.

(c) Radiation Effects

Considering the low temperature at which these tests were conducted ($T_o \sim 800^\circ\text{R}$, $T_w \sim 200\text{-}300^\circ\text{R}$), the estimated error due to radiation effects is less than 1%.

(d) Surface Curvature

The error in neglecting the local curvature of the wall is proportional to $\left| -\delta/R_N + (\delta/R_N)^2 \right|$. For this geometry the error is approximately -1%.

(e, f) Nonuniform Precooling and Shear Layer Heating

The correction of the data for errors due to initial transient conduction effects was performed using the Thomas-Fitzsimmons⁹ (T-F) method described in Appendix C. These initial transient conduction effects occur due to the nonuniform precooling of the model and the nonuniform heating of the model as it was injected through the tunnel free shear layer into the test section.

At the start of each test, the tunnel was evacuated to 10 Torr in order to boil off any moisture present and avoid the possibility of any condensation on the model surface. Once this was accomplished, the pressure was raised to 100 Torr and the model was cooled to a uniform temperature of 105°R. Before the pressure was lowered to 5 Torr in order to begin the tunnel starting sequence, the cooling had to be terminated in order to avoid any solidification of the liquid nitrogen as it expanded through the cooling nozzles. Thus, during the period that the tunnel pressure was being lowered to 5 Torr and the time required to start the other equipment used to support the flow once it was established, the model was nonuniformly heated. An additional nonuniform heating of the model occurs once it leaves the cooling chamber and before it is exposed to the test stream, since the model must be passed through the free shear layer of the open jet tunnel before it enters the test core.

(g) Thermocouple Losses

Small diameter (0.005 in.) chromel-alumel thermocouples were used in order to reduce any associated conduction losses. They were welded tangent to the surface, since

tests conducted by Wilson⁸ showed that this reduced the error significantly, as opposed to the error which would occur if they were welded normal to the surface. The T-F method was used to correct the data for transient errors arising from the initial transient effects associated with the presence of the thermocouple. The corresponding steady state error is presently being measured for a typical condition and will be reported in Ref. 10.

(h) Conduction Errors

(1) Normal Conduction

Since the wall is of finite thickness, there is always a gradient in the normal direction. Since the backface temperature is actually measured, the data must be corrected for errors resulting from the existence of this temperature gradient. The correction for steady state error associated with this effect was obtained using a one-dimensional result derived in Ref. 30 of the form

$$\frac{h_a}{h} = 1 + \frac{\lambda}{3} + \frac{2\lambda^2}{15} + \dots \quad (B-5)$$

where $\lambda = h\delta/k_m$ and h_a is the corrected heat transfer coefficient.

The model wall thickness was chosen to be nominally 0.025 in., as compromise between structural integrity and minimizing any associated conduction losses. The specific magnitude of the correction as obtained using Eq. (B-5) depends upon the level of the local heat transfer. For the tests described in this report, the

maximum correction was on the order of 2 to 3%. The correction for the initial transient conduction error associated with the initial normal conduction through the model skin as the model first senses the free-stream flow was obtained using the T-F method.

(2) Longitudinal Conduction

The longitudinal gradients on the conical surface are small even at the higher angles of attack. Thus, the associated impressed conduction effects should be very small. The corresponding gradients on the spherical cap are large, but in most regions the large size of the model results in relatively small conduction errors for the test times ($t < 2$ sec) used in the data reduction. These errors were estimated, using a technique similar to that discussed in Ref. 8, to be on the order of 1 to 2% for the test times encountered. However, in regions where the heat transfer distribution is somewhat discontinuous (transition points, sphere cone juncture), the conduction errors are larger. None of these errors is accounted for in the final data reduction, but they are estimated to be less than 5% for the current test conditions.

(3) Circumferential Conduction

At angle of attack, the circumferential gradients can become quite large. However, since the model is quite large, the errors are small for the specific thermocouple layout and test times used in these tests. They were estimated on the conical surface, using a procedure similar to that described in Ref. 8, to be less than 1% for the specific thermocouple

locations and test times used in the data reduction. The gradients on the sphere are smaller, but the surface area is also smaller. A similar estimate in this region also yielded errors on the order of 1%, except near the stagnation region where the error is much larger (~5-10% at the higher angles of attack).

(i) Stepwise Integration Technique

In order to determine the effect of the specific interval Δt on the data reduction, tests were conducted with recording intervals of 0.28 and 0.10 sec at the same freestream conditions. A comparison of the two resultant distributions showed very good agreement. All the data contained in this report were reduced from transient temperature data recorded at time intervals of 0.28 sec.

The linear fit of C_p over the small temperature ranges encountered in any time interval was also found to be a good approximation.

APPENDIX C

THOMAS-FITZSIMMONS CONDUCTION CORRECTION METHOD

Conduction within the thin wall of the model occurs whenever there are local temperature gradients. The thin-skin calorimeter technique ignores any of these effects and, thus, the data reduced using that technique must be corrected for any subsequent errors arising from this assumption.

A method was developed by Thomas and Fitzsimmons in Ref. 9 which corrects the subsequent data for the initial transient conduction errors that decay rapidly in time. Individual thermocouple data are used directly in this technique as opposed to other techniques which calculate $\nabla^2 T$, thereby needing other closely spaced thermocouples surrounding the one of interest. This latter technique is sensitive to the accuracy of the respective thermocouple readouts and is subject to large errors in the calculated correction, unless these measurements are very accurate. It also requires many more thermocouples for a single measurement. However, it should be pointed out that this technique, if accurate, corrects for steady state as well as transient errors, whereas the T-F method only corrects the data for errors arising from initial transient conduction effects which decay rapidly in time.

Estimates of the steady state errors, for the test times used in the data reduction, indicate that these errors are not large and are much smaller than the initial transient conduction errors which occur during the test. Since only the initial aerodynamic heat transfer is of interest, the T-F method was used to correct the data. This choice was reinforced by the fact that it was easier to apply and more straightforward than other approaches. It is tailored to correct for initial errors arising from nonuniform precooling, nonuniform heating while passing through the shear layer, initial transient

Preceding page blank

normal conduction, and initial transient errors arising from the presence of the thermocouple.

Thomas and Fitzsimmons demonstrated that by curve fitting the individual thermocouple data after the initial transient conduction was minimal and before the impressed conduction effects became important, the correct heat transfer coefficient could be obtained by a backward extrapolation in time to the initial starting time. Actual choices of the specific time interval over which the data should be fit is subject to a judgment regarding the specific test data to which the method is being applied. In these tests, for ease of computation, due to the volume of test data to be reduced, various specific time intervals were chosen and a quadratic least-squares fit was obtained over the intervals, using six to eight points. The specific interval chosen for a given test and thermocouple was selected from the time history plots of the heat transfer coefficient. It was also found to be necessary to check each curve fit individually and to make refinements where necessary in order to obtain adequate curve fits to the data.

REFERENCES

1. Widhopf, G. F., "Turbulent Heat Transfer Measurements on a Blunt Cone at Angle of Attack," TR-0059(S6816-66)-1, Feb. 1971, The Aerospace Corp., San Bernardino, Calif.; also presented at the AIAA 9th Aerospace Sciences Meeting, Jan. 1971, Preprint No. 71-36; also AIAA Journal, Vol. 9, No. 8, Aug. 1971, pp. 1574-1580.
2. Zakkay, V. and Sakell, L., "Laminar, Transition and Turbulent Heat Transfer to the Leeward Side of Axially Symmetric Bodies," New York University, to be published.
3. Widhopf, G. F., "Heat Transfer Correlations for Blunt Cones at Angle of Attack," TR-0172(S2816-63)-1, July 1971, The Aerospace Corp., San Bernardino, Calif.; also Journal of Spacecraft and Rockets, Vol. 8, No. 9, Sept. 1971, pp. 1002-1004.
4. Geinader, F., Schlesinger, M. I., Baum, G., and Cornett, R., "The U.S. Naval Ordnance Laboratory Hypersonic Tunnel," NOLTR 67-27, Apr. 1967, U.S. Naval Ordnance Laboratory, White Oak, Maryland.
5. Baltakis, F. P., "Performance Capability of the NOL Hypersonic Tunnel," NOLTR 68-187, Oct. 1968, U. S. Naval Ordnance Laboratory, White Oak, Maryland.
6. Willis, J. W., "DARE II Data Acquisition and Recording Equipment for the U.S. Naval Ordnance Laboratory's Hypersonic Tunnel No. 8," NOLTR 63-281, 1964, U.S. Naval Ordnance Laboratory, White Oak, Maryland.
7. Wilson, D. M., and Fisher, P. D., "Measurements of Hypersonic Turbulent Heat Transfer on Cooled Cones," Proc. 1966 Heat Transfer and Fluid Mech. Inst., Stanford University Press, 1966.
8. Wilson, D. M., "The Prediction of Errors and the Improvement of Data Obtained in Wind-Tunnel Heat-Transfer Tests," NOLTR 70-197, Sept. 1970, U.S. Naval Ordnance Laboratory, White Oak, Maryland.
9. Nagel, A. L., Fitzsimmons, H. D., and Doyle, L. B., "Analysis of Hypersonic Pressure and Heat Transfer Tests on Delta Wings with Laminar and Turbulent Boundary Layers," NASA CR-535, Aug. 1966, The Boeing Co., Seattle, Wash.

10. NOL report to be published.
11. Risher, D. B., "Multiple Pressure Transducer Banks and Their Application," NOLTR 67-148, 1967, U.S. Naval Ordnance Laboratory, White Oak, Maryland.
12. Abbett, M. J., and Fort, R., "Three-Dimensional Inviscid Flow about Supersonic Blunt Cones at Angles of Attack, III: Coupled Subsonic and Supersonic Programs for Inviscid Three-Dimensional Flow," Sandia Laboratories SC-Cr-68-3728, Sept. 1968, General Applied Science Laboratories, Westbury, N.Y.
13. Fay, J. A., and Riddell, F. R., "Theory of Stagnation Point Heat Transfer in Dissociated Air," Journal of the Aeronautical Sciences, Vol. 25, No. 2, Feb. 1958, pp. 73-85.
14. Mateer, G. G., "Effects of Wall Cooling and Angle of Attack on Boundary Layer Transition on Sharp Cones at $M = 7.4$," NASA Ames Research Center, Moffett Field, Calif.; presented at the Boundary Layer Transition Specialists Workshop, held at The Aerospace Corp., San Bernardino, Calif. 3-5 Nov. 1971.
15. Mateer, G. G., and Larson, H. K., "Unusual Boundary Layer Transition Results on Cones in Hypersonic Flow," AIAA Journal, Vol. 7, No. 4, Apr. 1969, pp. 660-664.
16. Otis, J. H., Jr., et al., "Strategic Reentry Technology Program (STREET-A), Final Report, Vol. II," AVSD-0210-70-RR, Vol. II, SAMSO TR-70-247, Vol. II, Nov. 1970, Avco Systems Division, Wilmington, Mass.
17. Vaglio-Laurin, R., "Laminar Heat Transfer on Three-Dimensional Blunt Nosed Bodies in Hypersonic Flow," American Rocket Society Journal, Vol. 29, No. 2, Feb. 1959, pp. 123-129.
18. Chen, K. K., and Tyson, N. A., "Extension of Emmons' Spot Theory to Flows on Blunt Bodies," AIAA Journal, Vol. 9, No. 5, May 1971.
19. Vaglio-Laurin, R., "Turbulent Heat Transfer on Blunt-Nosed Bodies in Two-Dimensional and General Three-Dimensional Hypersonic Flow," Journal of the Aerospace Sciences, Vol. 27, No. 1, Jan. 1960, pp. 27-36.
20. McCuen, P. A., Schaefer, J. W., Lundberg, R. E., and Kendall, R.M., "A Study of Solid-Propellant Rocket Motor Exposed Material Behavior," Final Report No. 149, Feb. 1965, Vidya Division, Itek Corp.

21. Walker, G. K., "A Particular Solution to the Turbulent Boundary Layer Equation," Journal of the Aerospace Sciences, Vol. 27, No. 9, Sept. 1960.
22. DeJarnette, F. R., and Tai, T. C., "A Method for Calculating Laminar and Turbulent Convective Heat Transfer over Bodies at an Angle of Attack," NASA CR-101678, Mar. 1969, Virginia Polytechnic Institute, Blacksburg, Virginia.
23. Sanlorenzo, E. A., "Method for Prediction of Streamlines and Heat Transfer to Bodies in Hypersonic Flow," GASL TR No. 177, July 1960, General Applied Science Laboratories, Westbury, N.Y.; also, "Method for Calculating Surface Streamlines and Laminar Heat Transfer to Blunted Cones at Angle of Attack," Journal of the Aerospace Sciences, Vol. 28, No. 11, Nov. 1961, pp. 904-905.
24. Vasiliu, J., "Calculation of Surface Streamlines and Laminar Heat Transfer Rates for Blunt Cones in Three-dimensional Flow," ATM-66(6560)-11, July 1965, The Aerospace Corp., San Bernardino, Calif.
25. Cebeci, T., and Smith, A. M. O., "A Finite Difference Method for Calculating Compressible Laminar and Turbulent Boundary Layers," Journal of Basic Engineering, Vol. 92, No. 3, Sept. 1970, pp. 523-535.
26. Bushnell, D. M., Jones, R. A., and Huffman, J. K., "Heat Transfer and Pressure Measurements on Spherically Blunted 25° Half Angle Cone at Mach 8 and Angles of Attack up to 90°," NASA Technical Note TN-D-4792, Oct. 1968, NASA Langley Research Center, Hampton, Virginia.
27. Beckwith, I. E., and J. J. Gallagher, "Heat Transfer and Recovery Temperatures on a Sphere with Laminar, Transitional, and Turbulent Boundary Layers at Mach Numbers of 2.00 and 4.15," NACA TN 4125, 1957.
28. Stetson, K. F., "Boundary-Layer Transition on Blunt Bodies with Highly Cooled Boundary Layers," Journal of Aerospace Sciences, Vol. 27, 1960, p. 81.
29. Bandettini, A., and Isler, W. E., "Boundary-Layer Transition Measurements on Hemispheres of Various Surface Roughnesses in a Wind Tunnel at Mach Numbers from 2.48 to 3.55," NASA Memo 12-25-58A, 1959.
30. Naysmith, A., "Measurements of Aerodynamic Heat Transfer in Intermittent Wind Tunnels," R.A.E. T.N. Aero. 2942, Bedford, England, Jan. 1964.